ELECTROSPRAY: FROM IONS IN SOLUTION TO IONS IN THE GAS PHASE, WHAT WE KNOW NOW

Paul Kebarle[1]* and Udo H. Verkerk[2]
[1]*Department of Chemistry, University of Alberta, Edmonton, Alberta, Canada T6G 2G2*
[2]*Centre for Research in Mass Spectrometry CB 220, Chemistry Building, York University, 4700 Keele Street, Toronto, Ontario, Canada M3J 1P3*

Received 23 November 2008; received (revised) 15 February 2009; accepted 15 February 2009

Published online 23 June 2009 in Wiley InterScience (www.interscience.wiley.com) DOI 10.1002/mas.20247

There is an advantage for users of electrospray and nanospray mass spectrometry to have an understanding of the processes involved in the conversion of the ions present in the solution to ions in the gas phase. The following processes are considered: Creation of charge droplets at the capillary tip; Electrical potentials required and possibility of gas discharges; Evolution of charged droplets, due to solvent evaporation and Coulomb explosions, to very small droplets that are the precursors of the gas phase ions; Production of gas phase ions from these droplets via the Ion Evaporation and Charge residue models; Analytical uses of ESIMS of small ions, qualitative and quantitative analysis; Effects of the ESI mechanism on the analysis of proteins and protein complexes; Determination of stability constants of protein complexes; Role of additives such as ammonium acetate on the observed mass spectra. © 2009 Wiley Periodicals, Inc., Mass Spec Rev 28:898–917, 2009
Keywords: *ESIMS; nano-ESIMS; mechanisms ESIMS; protein complexes; ion evaporation model; charge residue model; multiply charged proteins*

I. INTRODUCTION

This work is addressed to users of ESIMS. It is intended for those just entering the field and more advanced users. Understanding of ''how it all works'' is desirable because the mass spectra that one observes depend on a large number of parameters: choice of solvent and concentrations of the analyte, choice of additives to the solution that may be beneficial, choice of the flow rates of the solution through the spray capillary, the electrical potentials applied to the spray capillary (also called ''needle'') and the potentials on the electrodes leading to the mass analysis. The choice of these parameters requires not only some understanding of conventional mass spectrometry but also of the electrospray mechanism. In early work on ESIMS many of the parameters were established experimentally by trial and error but now that a better understanding of the mechanism is at hand, one can make more rational choices for the conditions most suited for a given ESI analysis.

Correspondence to: Paul Kebarle, Department of Chemistry, University of Alberta, Edmonton, Alberta, Canada T6G 2G2.
E-mail: paul.kebarle@ualberta.ca

Remarkably ESI can handle a vast variety of analytes such as inorganic ions as well as ionized polymers, nucleic acids, peptides and proteins that have a molecular mass from kilo- to hundreds of mega-Daltons. The analytes present in the solution may be ions, such as the inorganic metal ions M^+ and M^{2+} or negative ions such as the halide ions X^- or sulfates SO_4^{2-}. They also can be compounds that are not ionized in the solution that is sprayed. In that case the analyte is charged by association with one or more of the ions present in the solution. This charging process is part of the electrospray mechanism.

A very recent and exciting area is the study via ESIMS of homogeneous catalysis in solution of polymerization reactions that involves the detection of the ionic reaction intermediates containing the ionic catalyst (Zhang, Chen, & Chen, 2004; di Lena, Quintanilla, & Chen, 2005; Santos & Metzger, 2006).

Readers interested in a more extended analysis of ESIMS will find the work of Cech and Enke (2001a) of great value.

ESIMS is the brainchild of Malcolm Dole. In the 1960s, Dole was very interested in the determination of the molecular mass of synthetic polymers such as polystyrene and the development of a technique with which this could be done by mass spectrometry. To do this one had to find a method for the transfer of these non-volatile solids into the gas phase and also charge them. He discovered the existence of electrospray by accident while visiting a car manufacturer where cars were painted by electrospray. Electrospray (ES) produced very small charged droplets of paint which were attracted to the metal surface of the car. Using ES with a solution of the polystyrenes Dole and co-workers were able to develop apparatus that produced charged polystyrene molecules in the gas phase with molecular mass in the kilo-Dalton range (Dole et al., 1968). However there were some ambiguities in the interpretation of Dole's results. John Fenn applied ESI to solutions of salts in methanol and of small ions and, using a quadrupole mass spectrometer, was able to demonstrate the ability of ESI to produce positive and negative ions in the gas phase (Yamashita & Fenn 1984a,b). Subsequent work by Fenn and co-workers (Whitehouse et al., 1985) clearly demonstrated that ESIMS could be used very effectively for the analysis of peptides and proteins with molecular mass in the kilo-Dalton range. The detection of very high molecular mass compounds with mass spectrometers of modest mass to charge (m/z), range due to multiple charges z on the analyte was demonstrated in that work. Subsequent work demonstrated that molecular masses as high as five million became accessible due to multiple charging

(Takahashi & Fenn, 1992). This work initiated the ESIMS revolution that is continuing to this day.

II. FORMATION OF GAS PHASE IONS

A. Major Stages in ESI

There are three major steps in the production of gas-phase ions from electrolyte ions in solution: (a) production of charged droplets at the ES capillary tip; (b) shrinkage of the charged droplets due to solvent evaporation and repeated charge-induced droplet disintegrations leading ultimately to very small highly charged droplets capable of producing gas-phase ions; (c) the actual mechanism by which gas-phase ions are produced from these droplets. The stages (a) to (c) occur in the atmospheric pressure region of the apparatus (see Fig. 1).

Some of the ions resulting from the preceding stages (a–c) enter the vacuum region of the interface leading to the mass spectrometer. This interface is either a very small orifice or a capillary. An apparatus using a capillary is shown in Figure 2a,b. The ions entering through the capillary may be clustered with solvent molecules and other additives and are subjected to a thermal declustering ''clean up'' by heating of the capillary. The chamber past the capillary is at a partial vacuum (pressure of a few torr). A second clean up is obtained by collisional activation by applying an electric potential difference between the capillary exit and the skimmer leading to the second (high vacuum) chamber that is the housing of the mass spectrometer.

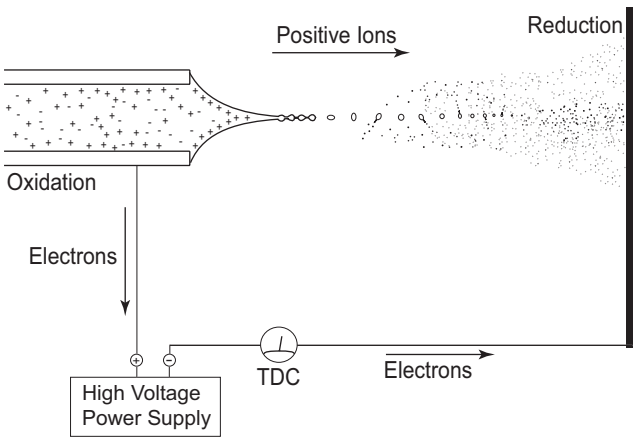

FIGURE 1. Illustration of major processes in the atmospheric pressure region of an ESI ion source run in the positive ion mode. Penetration of the imposed electric field into the liquid leads to an enrichment near the meniscus of positive ions present in the solution. This causes a destabilization of the meniscus and formation of a cone and a jet charged by an excess of positive ions. The jet splits into droplets charged with an excess of positive ions. Evaporation of the droplets brings the charges closer together. The increasing Coulombic repulsion destabilizes the droplets which emit jets of charged progeny droplets. Evaporation of progeny droplets leads to emission of second generation progeny droplets, and so on until free gas-phase ions form at some point. TDC stands for total droplet current (I).

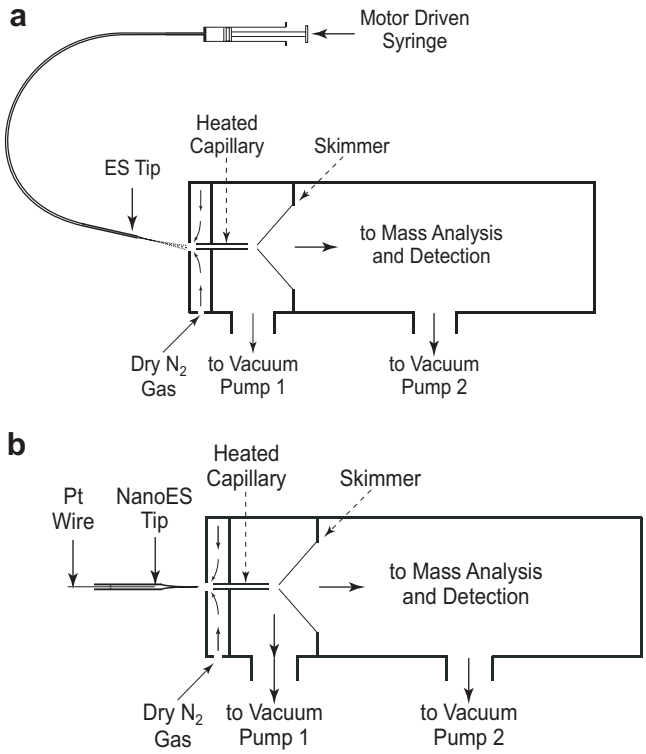

FIGURE 2. **a**: Electrospray ion source and interface to mass spectrometer. Solution containing analyte is supplied to the metal ES spray tip by syringe via a flexible glass capillary. A positive potential is applied to the spray tip (positive ion mode). Positively charged droplets emerge from the spray capillary tip (see Fig. 1). Solvent evaporation of the charged droplets leads to gas-phase ions. A mixture of ions, small charged droplets and solvent vapor in the ambient gas enters the orifice leading to the nitrogen countercurrent chamber. The weak nitrogen counterflow removes solvent vapor. The ions, driven by an electric potential and pressure difference, enter the low pressure chamber through the heated capillary. An electric field between the capillary and the skimmer accelerates the ions for a further collision activated ''clean-up'' of the ions. **b**: Same as (a) but for nanoelectrospray. The large diameter end of the Nano-ES tip capillary was ''loaded'' with μL amounts of solution. The electrical potential is applied to the Nano tip either by a Pt wire as shown in the figure, or by a metal film coating the outside of the capillary.

B. Generation of the Charged Droplets at the ES Capillary Tip

As shown in Figure 1, a voltage V_c, of 2–3 kV, is applied to the spray capillary. Typically the capillary is 1 mm o.d. and located 1–3 cm from the counterelectrode. The counterelectrode in ESMS may be a plate with an orifice leading to the mass spectrometric sampling system, or a sampling capillary mounted on the plate which leads to the MS as shown in Figure 2a. Because the spray capillary tip is very thin, the electric field E_c at the capillary tip is very high ($E_c \approx 10^6$ V/m). The value of the field at the capillary tip opposite a large and planar counterelectrode can be estimated with the approximate relationship (Loeb et al., 1941):

$$E_c = \frac{2V_c}{r_c \ln(4d/r_c)} \quad (1)$$

where V_c is the applied potential, r_c the capillary outer radius, and d the distance from capillary tip to the counterelectrode. For example, the combination $V_c = 2{,}000$ V, $r_c = 5 \times 10^{-4}$ m, $d = 0.02$ m leads to $E_c \approx 1.6 \times 10^6$ V/m. The field E_c is proportional to V_c and the most important geometry parameter is r_c. E_c is essentially inversely proportional to r_c, but decreases very slowly with the electrode separation d due to the logarithmic dependence on d. For potentials required for electrospray, see Section IID.

A typical solution supplied to the capillary is a polar solvent in which the analyte is soluble. Because ESIMS is a very sensitive method, very low concentrations, 10^{-7}–10^{-3} mol/L (M) of analyte can be used. Methanol or methanol–water, acetonitrile or acetonitrile–water are often used as the solvent. Because electrolyte concentrations as low as 10^{-7} M are sufficient for ESI to function other solvents such as toluene that have very low solubility for electrolytes, can be also used. For simplicity, the subsequent discussion will assume that the analyte is ionic. Only the positive ion mode will be considered.

The field E_c, when turned on, will penetrate the solution. The field will be highest near the spray capillary tip. This will cause a polarization of the solvent near the meniscus of the liquid. In the presence of even traces of an electrolyte the solution will be sufficiently conducting and the positive and negative electrolyte ions in the solution will move under the influence of the field. This will lead to an enrichment of positive ions near the surface of the meniscus and negative ions away from the meniscus. The downfield forces due to the polarization cause a distortion of the meniscus into a cone pointing downfield (see Fig. 1). The increase of surface due to the cone formation is resisted by the surface tension of the liquid. The cone formed is called a Taylor cone (Taylor, 1965; Fernandez de la Mora, 2007). If the applied field is sufficiently high the tip becomes unstable and a fine jet emerges from the cone tip. The surface of the jet is charged by an excess of positive ions. The repulsion between the charges on the jet causes the jet to break up into small charged droplets (see Figs. 1 and 3a) (Cloupeau, 1994; Cloupeau & Prunet-Foch, 1994).

It is indicated in Figure 3a that the size of the droplets formed from the cone jet is dependent on the jet diameter $2R_J$ suggesting that the majority of the droplets produced would be approximately of the same size, that is, approximately monodisperse. This was proposed by Cloupeau (1994) and confirmed by studies of Tang and Gomez (1995). Shown also is a much smaller satellite droplet.

The droplets are positively charged due to an excess of positive electrolyte ions at the surface of the cone and the cone jet. Thus, if the major electrolyte present in the solution was ammonium acetate, the excess positive ions at the surface will be mostly NH_4^+ ions. The charged droplets drift downfield through the air towards the opposing electrode. Solvent evaporation at constant charge leads to droplet shrinkage and an increase of the electric field normal to the surface of the droplets. At a given radius the increasing repulsion between the charges overcomes the surface tension at the droplet surface. This causes a coulomb fission of the droplet, also called a coulomb explosion. The

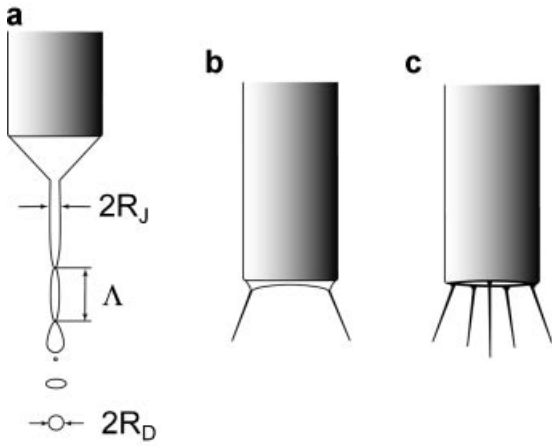

FIGURE 3. Different forms of Electrospray at the tip of the spray capillary. Cone jet mode (**a**) and multi-jet modes (**b**) and (**c**). Relationship in cone jet mode between radius of droplets and radius of jet: $R_D/R_J \approx 1.9$ (after Cloupeau, 1994, see text).

droplet fission occurs via formation of a cone and a cone jet that splits into a number of small progeny droplets. This process bears close resemblance to the cone jet formation at the capillary tip (see Fernandez de la Mora, 2007) and references therein. Further evaporation of the parent droplet leads to repeated fissions. The progeny droplets also evaporate and undergo fission. More details on these processes are given in Section IIE. Very small charged droplets result that lead ultimately to gas-phase ions by processes which will be described in detail in subsequent sections.

More recent studies by Vertes and co-workers (Marginean et al., 2004) using fast time-lapse imaging of the Taylor cone provide details on the evolution of the Taylor cone into a cone jet and pulsations of the jet. These pulsations lead to spray current oscillations. The current oscillations are easy to determine with conventional equipment and can be used as a guide for finding conditions that stabilize the jet and improve signal-to-noise ratios of the mass spectra. The cone-jet mode is most often used in ESIMS. It is also the best-characterized mode in the electrospray literature. While some of the other modes have been and are being used for ESIMS, it appears that the cone jet mode is the most efficient mode.

C. Electrospray as a Special Electrolytic Cell

At a steady operation of the electrospray in the positive ion mode (see Fig. 1) the positive droplet emission continuously carries off positive charge. The requirement for charge balance in such a continuous electric current device, together with the fact that only electrons can flow through the metal wire supplying the electric potential to the electrodes (Fig. 1), leads to the conclusion that the ES process must include an electrochemical conversion of ions to electrons. In other words, the ES device can be viewed as a special type of electrolytic cell (Blades, Ikonomou, & Kebarle, 1991). It is special because the ion transport does not occur through uninterrupted solution, as is normally the case in electrolysis. Part of the ion transport occurs through the gas phase. Thus, in the

positive ion mode where positively charged droplets and later positive gas-phase ions are the charge carriers, a conventional electrochemical oxidation reaction should be occurring at the positive electrode, that is, at the liquid/metal interface of the spray capillary (Fig. 1). This reaction supplies the extra positive ions to the solution that prevents the build-up of a charge imbalance. The nature of these ions depends on the experimental conditions. If the spray capillary is made of metal, metal ions could be entering the solution causing a release of electrons to the metal electrode (see Eq. 2). The other alternative for producing extra positive ions is the removal of negative ions present in the solution by an oxidation reaction as illustrated below (Eq. 3) for aqueous solutions:

$$M(s) \rightarrow M^{2+}(aq) + 2e(\text{onmetalsurface}) \quad (2)$$

$$4OH^{-}(aq) \rightarrow O_2(g) + 2H_2O + 4e(\text{onmetalsurface}) \quad (3)$$

One expects that the reaction with the lowest oxidation potential will dominate, and that such a reaction will be dependent on the material present in the metal electrode, the ions present in the solution and the nature of the solvent. Proof for the occurrence of an electrochemical oxidation at the metal capillary was provided by Blades, Ikonomou, and Kebarle (1991).

Van Berkel and co-workers, in a series of publications, have examined the consequences of the electrochemical processes to ESIMS. For example, they were able to demonstrate that ions produced by the electrolysis process, such as hydrogen ions, can in some cases have important effects on the mass spectra obtained with pH sensitive analytes such as non-denatured proteins (Van Berkel, Zhou, & Aronson, 1997).

D. Required Electrical Potentials for ESI Can Cause Electrical Gas Discharges

Smith (1986) was able to derive a very useful approximate equation for the potential, V_{on}, required for the onset of electrospray (see Eq. 4) where γ is the surface tension of the solvent, ε_o the permittivity of vacuum, r_c the radius of the capillary, and θ the half angle of the Taylor cone.

$$V_{on} \approx \left(\frac{r_c \gamma \cos\theta}{2\varepsilon_o}\right)^{1/2} \ln\left(\frac{4d}{r_c}\right) \quad (4)$$

Substituting the values $\varepsilon_o = 8.8 \times 10^{-12}\,J^{-1}\,C^2$ and $\theta = 49.3^\circ$ (see Taylor, 1965) one obtains:

$$V_{on} = 2 \times 10^5 (\gamma r_c)^{1/2} \ln\left(\frac{4d}{r_c}\right) \quad (5)$$

where γ must be substituted in N/m (Newton/meter) and r_c in m to obtain V_{on} in volts. Shown in Table 1 are the surface tension values for four solvents and the calculated electrospray onset potentials for $r_c = 0.1$ mm and $d = 40$ mm. The surface of the solvent with the highest surface tension (H_2O) is the most difficult to stretch into a cone and jet, and this leads to the highest value for the onset potential V_{on}.

Experimental verification of Equation (4) has been provided by Smith (1986), Ikonomou, Blades, and Kebarle (1991), and Wampler, Blades, and Kebarle (1993). For stable ES operation one needs to go a few hundred volts higher than V_{on}. Use of neat water as the solvent can lead to the initiation of an electric discharge from the spray capillary tip, particularly when the capillary is negative, that is, in the negative ion mode. The electrospray onset potential V_{on} is the same for both the positive and negative ion modes; however, the electric discharge onset is lower when the capillary electrode is negative and metallic (Ikonomou, Blades, & Kebarle, 1991; Wampler, Blades, & Kebarle, 1993). This is probably due to emission of electrons from the negative capillary which initiate the discharge.

The occurrence of an electric discharge leads to an increase of the capillary current (I). Currents above 10^{-6} A are generally due to the presence of an electric discharge. A much more specific test is provided by the appearance of discharge-characteristic ions in the mass spectrum. Thus, in the positive ion mode the appearance of protonated solvent clusters such as $H_3O^+(H_2O)_n$ from water or $CH_3OH_2^+(CH_3OH)_n$ from methanol indicates the presence of a discharge (Ikonomou, Blades, & Kebarle, 1991). Protonated solvent ions are produced at high abundance by ES in the absence of a discharge only when the solvent has been acidified, that is, when H_3O^+ and $CH_3OH_2^+$ are present in the solution.

The presence of an electric discharge degrades the performance of ESMS, particularly so at high discharge currents. The Electrospray ions are observed at much lower intensities than was the case prior to the discharge, while the discharge-generated ions appear with very high intensities (Ikonomou, Blades, & Kebarle, 1991; Wampler, Blades, & Kebarle, 1993).

The high potentials required for electrospray show that air at atmospheric pressure is not only a convenient but also a very suitable ambient gas for ES, particularly when solvents with high surface tension, such as water, are to be electrosprayed. The oxygen molecules in air have an appreciable electron affinity and readily capture free electrons. Initiation of gas discharges occurs when free electrons present in the gas (due to cosmic rays or background radiation) are accelerated by the high electric field near the capillary to velocities where they can ionize the gas molecules.

TABLE 1. Approximate required onset voltages*, V_{on} for ESI of solvents with different surface tension γ

Solvent	CH_3OH	CH_3CN	$(CH_3)_2SO$	H_2O
γ (N/m)	0.0226	0.030	0.043	0.073
V_{on}(Volt)	2200	2500	3000	4000

*Calculated with Equation (4) for a spray tip of 0.1 mm radius at a distance of 4 cm from tip of needle to a negative electrode such as the metal plate with orifice leading to the vacuum of the mass spectrometer.

The presence of gases that have higher electron affinity than O_2 and have higher electron capture cross sections will lead to electron capture even when present at much lower concentrations than O_2, and can suppress the electrical breakdown. SF_6 and polychlorinated hydrocarbons are such gases. SF_6 has been used to advantage for the suppression of discharges in electrospray. Use of these trace gas additives prevents gas discharges even when neat water is used as solvent (Ikonomou, Blades, & Kebarle, 1991; Wampler, Blades, & Kebarle, 1993). However, the use of small amounts of gases like SF_6, can introduce foreign ions such as F^- into the observed mass spectrum. The production of F^- was observed but due to the low m/z of this ion there is was no significant interference with the analyte ions.

E. Nanoelectrospray and Insights Into Fundamentals of Electrospray and Nanoelectrospray

Nanospray was developed by Wilm and Mann (1994, 1996). Their primary interest was an electrospray source for which much smaller quantities of analyte are required. Such a device would be particularly important for applications in biochemistry and the analysis of proteins where, in general, very small samples are available. With ESI, most of the analyte is wasted. The large diameter of the spray tip produces large droplets whose evolution to gas phase ions requires the presence of a large distance between the spray tip and the sampling orifice (or sampling capillary) (see Figs. 1 and 2a). As a result, only a very small fraction of formed gas phase ions is sampled by the orifice (capillary). With nanospray, the spray tip has a much smaller diameter resulting in a more efficient generation of gas phase ions (see Section IIG) so that the tip can be placed nearer to the sampling orifice resulting in more ions being sampled. In general, for non-viscous solutions the flow is not a forced flow, unlike the syringe driven flow as used in ESI (see Fig. 2a), and all of the solution to be sprayed is contained in the spray capillary whose entrance is left open. A ''self-flow'' results, which is due to the pull of the applied electric field on the solution at the capillary tip. The self-flow is controlled by the diameter of the capillary tip.

With nanospray one can use neat water as a solvent without causing electric gas discharges as is the case with electrospray (see Section 2D). Water as solvent is more suitable for the analysis of proteins which may denature in other solvents.

Nanoelectrospray has proven to be of enormous importance in the analysis of biochemical and (bio)pharmaceutical samples. For additional information on nanospray, see Juraschek, Dulks, and Karas (1999), Schmidt, Karas, and Dulks (2003), Chernushevich, Bahr, and Karas (2004).

F. Solvent Evaporation from Charged Droplets Causes Droplet Shrinkage and Fissions of Droplets

The charged droplets produced at the spray needle, shrink due to solvent evaporation while the charge remains constant. The energy required for the solvent evaporation is provided by the thermal energy of the ambient gas, air at atmospheric pressure in most cases. As the droplet gets smaller the repulsion between the charges at the surface increases and, at a certain droplet radius, this repulsion overcomes the cohesive force of the surface tension. An instability results and leads to fission of the droplet that typically releases a jet of small, charged progeny droplets. The condition for the instability, also called Coulomb fission, is given by the Rayleigh (1882) equation:

$$Q_{\mathrm{Ry}} = 8\pi(\varepsilon_0 \gamma R^3)^{1/2} \tag{6}$$

where Q_{Ry} is the charge on the droplet, γ the surface tension of the solvent, R the radius of the droplet, and ε_o the electrical permittivity. The shrinkage of the droplets at constant charge fission at or near the Rayleigh limit, and the release of a jet of small, monodisperse charged progeny droplets has been confirmed by a number of experiments. Most studies relevant to electrospray were done with Phase Doppler Interferometry (PDI). Recent PDI measurements by Beauchamp and co-workers (Grimm & Beauchamp, 2002; Smith, Flagan, & Beauchamp, 2002), are given in Table 2, together with results by other authors (Schweizer & Hanson, 1971; Richardson, Pigg, & Hightower, 1989; Taflin, Ward, & Davis, 1989). One can deduce from the table that the dependence on the type of solvent is relatively small. Thus, droplets from all solvents experience Coulomb fissions close to, or at, the Rayleigh limit given by Equation (6). The loss of mass on fission is less than 1% of the parent droplet but the loss of charge is much larger, that is, some 15–25% of the charge of the parent droplet.

Beauchamp and co-workers (Smith, Flagan, & Beauchamp, 2002) also provide information on the charge of the parent droplet immediately after the droplet fission. An example of such data is given in Figure 4, where the charge of the droplets before and after the fission is given as percent of the Rayleigh condition (Eq. 6). These, and results for the other solvents studied (Grimm & Beauchamp, 2002), show that the evaporating charged droplets oscillate at all times between fairly narrow limits of the Rayleigh limit. This finding has bearing on the discussion of the mechanism by which non-denatured proteins enter the gas phase (see Charged Residue Mechanism in Section IIJ).

When the sprayed solution also contains a solute such as a salt, at much higher concentration than the analyte, the continuous evaporation of the droplets will lead to very high concentrations of the salt and ultimately to charged solid particles—the ''skeletons'' of the charged droplets. These skeletons can reveal some aspects of the droplet evolution. Fernandez de la Mora and co-workers (Loscertales & Fernandez de la Mora, 1995; Gamero-Castano & Fernadez de la Mora, 2000a,b) have used this approach to study charged droplet evolution. This work is of special relevance to the ion evaporation model (IEM) and is discussed in Section IIG.

G. Evaporation of Droplets Leading to Coulomb Fissions Producing Progeny Droplets That Ultimately Lead to Ions in the Gas Phase

The process of repeated droplet fissions of parent droplets, leading to smaller parent droplets and progeny droplets, will ultimately lead to very small charged droplets that are the precursors of the gas-phase ions. The mechanisms by which the gas phase ions are produced from the very small ''final'' droplets

TABLE 2. Experimental observations of Rayleigh fissions of charged droplets

Reference	Solvent	Droplet diameter range (μm)[a]	Onset of Instability (% of Rayleigh limit)	% of mass lost in breakup[a]	% of charge lost in breakup
(Smith et al. 2002)	water	10 - 40	90	nd	20-40
	Methanol	10 - 40	110	"	15 - 20
	Acetonitrile	10 - 40	100	"	15 - 20
(Grimm & Beauchamp 2002)	n-heptane	35 - 45	100	"	19
	n-octane		87	"	17
	p-xylene		89	"	17
(Gomez & Tang 1994)	Heptane	20-100	70	nd	nd
(Taflin et al. 1989)	Low vapor pressure oils	4 - 20	75 - 85	2	10 - 15
(Richardson et al. 1989)	Dioctyl phtalate	nr	102 - 84	2.3	15 - 50
(Schweizer et al. 1971)	n-octanol	15 - 40	96 - 104	5	23

nr, not reported; nd, not determined.

is considered in Section IIH. Here we examine some of the details of the evolution of the initial droplets, formed at the spray capillary, to droplets that are the precursors of the ions. As will be shown below, a very large loss of solvent by evaporation occurs before formation of the final gas phase ions. It is desirable for certain applications of ESIMS to be able to estimate the increase of solute concentration due to evaporation.

A droplet evolution scheme is shown in Figure 5 that deals with droplets produced by nanoelectrospray. The nanospray droplets are very much smaller than the droplets produced by electrospray so that they reach the onset of gas phase ion creation much sooner.

The assumptions with which this scheme (Fig. 5) was obtained are described in detail in the Calculations and Experimental Section of Peschke, Verkerk, and Kebarle (2004). Water was used as solvent in the calculations. The calculations show that approximately 40% of the volume is lost between each droplet fission. A corresponding increase by 40% of the solute concentration must also occur. This means that after 10 successive fissions the parent droplet volume will decrease 29-fold and the concentration of solutes in the droplet will increase 29-fold. Such large increases in concentration when additives are initially present in millimolar concentrations may lead to saturation and, ultimately, solid residues before the parent droplets reach the size (see next section) required for the generation of gas phase ions. Thus most, if not all, of the ions observed must have been generated by the progeny droplets.

H. Mechanisms for the Formation of Gas-Phase Ions from Very Small and Highly Charged Droplets: The Ion Evaporation Model (IEM)

Two mechanisms have been proposed to account for the formation of gas-phase ions from the very small and highly charged droplets. The first mechanism was proposed by Dole who was interested in analytes of high molecular mass (Dole et al., 1968). For such macromolecules he assumed that, when very small droplets are formed by droplet evolution (see preceding section), some of these droplets would contain one analyte molecule as well as the ionic charges on the surface of the droplet. Solvent evaporation from such a droplet will lead to a gas-phase analyte ion whose charge originates from the charges at the surface of the vanished droplet. This assumption is now known as the charged residue model (CRM). The CRM is discussed in detail in Section IIJ.

Iribarne and Thomson (1976) and Thomson and Iribarne (1979) who worked with small ionic analytes such as Na^+ and Cl^-, proposed a different mechanism, the IEM. This model is discussed in the present section. The model predicts that direct ion emission from the droplets will occur after the radii of the droplets shrink to radii less than 10 nm. The ion evaporation process, by removing charge, replaces Coulomb fission.

Iribarne and Thomson supported their model by experimental results (Iribarne & Thomson, 1976) and theoretical calculations (Thomson & Iribarne, 1979). The experimental results involved measurements of the relative abundance of the

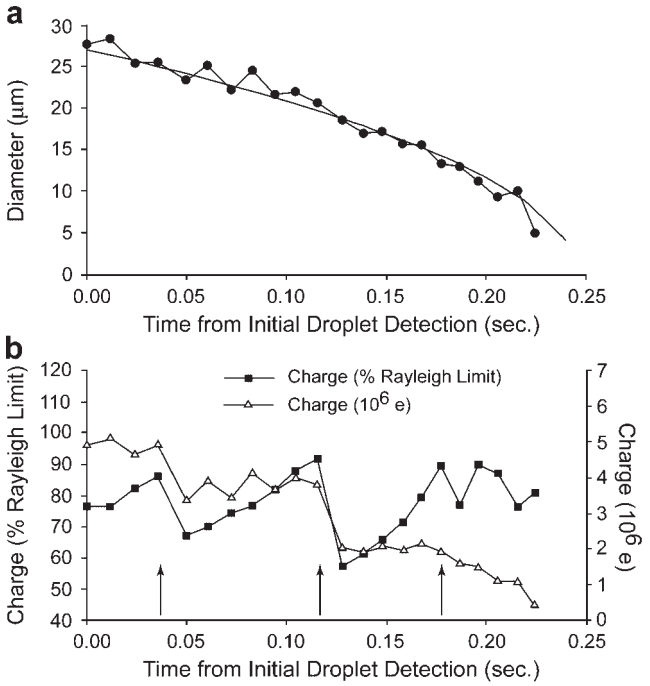

FIGURE 4. Evaporation and Coulomb fissions of one positively charged water droplet, in nitrogen gas at ambient pressure and 317 K. **a**: Observed diameter of droplet with time. Also shown (smooth curve) is the change of diameter due only to evaporation of a neutral water droplet in N_2 gas at 317 K. **b**: Variation of droplet charge with time. Arrows indicate discharge events. Coulomb fissions are observed at approximately 90% of the Rayleigh limit, and after the fission the droplet is at approximately 65% of the limit. (Reprinted from Smith, Flagan, & Beauchamp, 2002, with permission from the American Chemical Society, copyright 2002.)

ions produced by ESI of solutions containing NaCl as the only solute. The authors, examining the positive ions, found that there was a large number of ion aggregates of the type $[(NaCl)_n(Na)_m]^{m+}$, including $[(NaCl)_n(Na)]^+$, whose abundance decreased rapidly as n decreased. However, the lowest mass ion in that series, Na^+ (with $n=0$, $m=1$), and hydrated $Na(H_2O)_k^+$ (with $k=1$–3) had by far the highest abundances. This indicated to them that, while the large aggregate ions produced by ESI are probably due to a Charged Residue Mechanism type process, the abundant Na^+ and Na^+ hydrates must be due to a different mechanism where the Na^+ ions escape directly from the surface of the droplets. This ion escape process was called ion evaporation (Iribarne & Thomson, 1976). The authors also developed theoretical equations for the droplet conditions that will lead to ion evaporation (Thomson & Iribarne, 1979).

The theory leading to the equations predicting the conditions required for ion evaporation was based on the Transition State Theory used in reaction kinetics. The transition state of the ion evaporation reaction was evaluated with the assumption that the evaporating ion is one of the ionic charges at the surface of the droplet. The leaving ion is repelled by the Coulomb repulsion between it and the remaining charges on the droplet. But at very short distances from the droplet the leaving ion is also attracted to the droplet by the polarization of the droplet caused by the leaving ion. The ion–polarizability interaction is larger at very short distances from the droplet surface, while the repulsion becomes dominant at larger distances. The transition state is located where these two interactions become equal. The graphs in Figure 6 show the predicted radius at which droplet fission at the Rayleigh limit is replaced by ion evaporation. It indicates that the charged droplets must become very small, with a radius of approximately 100 Å (10 nm), before ion evaporation replaces droplet fission.

While Iribarne and Thomson's theory is plausible, not all assumptions need be correct. Therefore, several research groups have performed experiments to examine the predictions of the theory. Some of the most relevant work is due to Fernandez de la Mora and co-workers, who used an interesting approach to provide strong evidence for the qualitative validity of the ion evaporation mechanism. They circumvented the experimental difficulty of having to determine radius and charge of rapidly changing small evaporating droplets. Instead of concentrating on the evaporating droplets, they focused on the sizes and charges of the solid residues formed after evaporation of the solvent from the droplets. Since the solid residues had been "charged droplets" before the last of the solvent evaporated, the size and charge of these residues should represent to a fair approximation the sizes and charges of the final charged droplets. The solid residues, representing final droplets frozen in time, are amenable to measurement. This approach (Loscertales & Fernandez de la Mora, 1995; Gamero-Castano & Fernandez de la Mora, 2000a,b) provided results that were in good agreement with the IEM.

Theoretical work involving simulations of ion evaporation from charged droplets have also provided valuable insights into the IEM. A good example is the work by Vertes and co-workers (Znamenski, Marginean, & Vertes, 2003) on the evaporation of H_3O^+ ions from charged water droplets. Interested readers can observe the simulation of such ion evaporation at the website of Vertes: (http://www.gwu.edu/~vertes/publicat.html).

In summary, the IEM is experimentally well-supported for small (in)organic ions. However, the theoretical derivation of the model does not apply for very large ions such as proteins. For these macromolecular species, the CRM is much more plausible (see Section IIJ).

I. Experimental Determinations of the Sensitivity of Small Analytes (Presence of Other Solutes Can Decrease the Sensitivity of a Given Analyte. Surface Active Analytes Have High Sensitivities)

Practicing experimental mass spectrometrists using ESIMS for quantitative analysis need to know the dependence of the sensitivities of different ionic analytes on the nature of the analyte and possible interference due to the presence of other analytes or additives present in the solution. The analytes considered in this section are small inorganic ions that most likely enter the gas phase via the IEM.

An approximate equation for calculating the total droplet current I carried away by the droplets generated in the

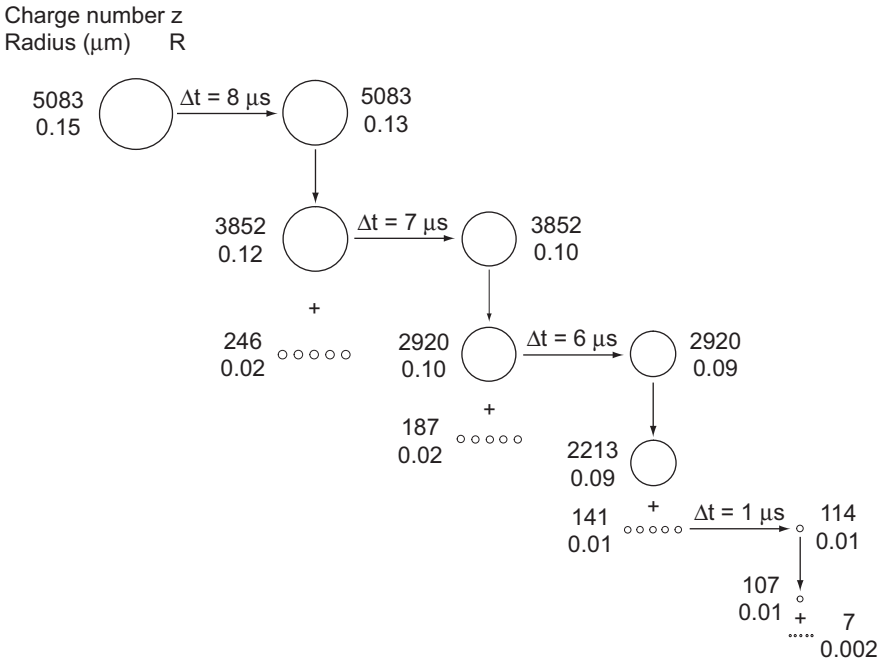

FIGURE 5. History of charged water droplets produced by nanospray. First droplet shown is a droplet produced at spray needle. The radius and charge of this droplet is followed in time for three evaporation and fission events. The first generation progeny droplets are shown as well as the fission of one of the progeny droplets that leads to second generation progeny droplets. *R* is the radius of the droplets and *Z* gives the number of charges on the droplet. The parent droplet charge is assumed to have $Z = 0.9\ Z_R$ just before the fission and $Z = 0.7\ Z_R$ just after the fission (as observed in Fig. 4), while the progeny droplets have $Z = 0.7\ Z_R$ just after the fission of the parent (based on data from Peschke, Verkerk, & Kebarle, 2004).

electrospray process was derived by Fernandez de la Mora and Locertales (1994) (see Eq. 7). The equation is based on experimental measurements of the current I and theoretical reasoning:

$$I = f\left(\frac{\varepsilon}{\varepsilon_0}\right)\left(\gamma K V_f \frac{\varepsilon}{\varepsilon_o}\right)^{1/2} \tag{7}$$

where γ is the surface tension of solvent, $\varepsilon/\varepsilon_o$ the dielectric constant of solvent, K the conductivity of solution, V_f the flow rate (volume/time), and $f(\varepsilon/\varepsilon_o)$ is a numerical function tabulated by the authors. The value of $f(\varepsilon/\varepsilon_o) \approx 18$ for liquids whose dielectric constant, $\varepsilon/\varepsilon_0 \geq 40$. This includes water $(\varepsilon/\varepsilon_o) = 78$ and water–methanol mixtures as well as acetonitrile and formamide. This relationship was obtained for solutions having conductivities (K) larger than $10^{-4}\,\mathrm{S\,m^{-1}}$. For polar solvents like water and methanol, and electrolytes that dissociate essentially completely to ions, this requirement corresponds to solutions with concentrations higher than $\sim 10^{-5}$ mol/L, that is, a concentration range that is often present in ESIMS. The flow rates used were below 1 μL/min and close to the flow rates used in conventional ESIMS. The equation is valid when the spray is operated in the cone jet mode.

Relevant to the present discussion is the dependence of I on the square root of the conductivity of the solution. At the low total electrolyte concentrations used in ESI, the conductivity is proportional to the concentration of the electrolyte. Thus, if a single electrolyte, E, was present in the solution, one would expect that the observed peak intensity, I_E, will increase with the square root of the concentration C_E.

In practice one seldom works with a single electrolyte system. Even with a single analyte ion A^+ there will be often also contaminating electrolytes E^+X^- present, for example Na^+ (from glassware). The presence of E^+ ions leads to two concentration regimes for the analyte:

(a) C_A much higher than C_E. In that case, the I_A is expected to increase with the square root of C_A.
(b) C_A much lower than C_E. In that case, I_A is expected to increase with the first power of C_A because now I_A will depend on a statistical competition between A^+ and E^+ for being surface charges on the droplets.

To cover both regions, Tang and Kebarle (1993) proposed Equation (8a) for a two-component system in the positive ion mode. Equation (8a) predicts that when C_E is much higher than C_A and constant, the observed ion current I_A will be proportional to C_A. In Equation (8), I is the total electrospray current leaving the spray capillary (that can be easily measured, see Fig. 1), p and f are proportionality constants (see Tang & Kebarle, 1993) while k_A, k_B are the sensitivity coefficients for A^+ and E^+. The magnitude of the sensitivity coefficients (k) will depend on the specific chemical ability of the respective ion species to

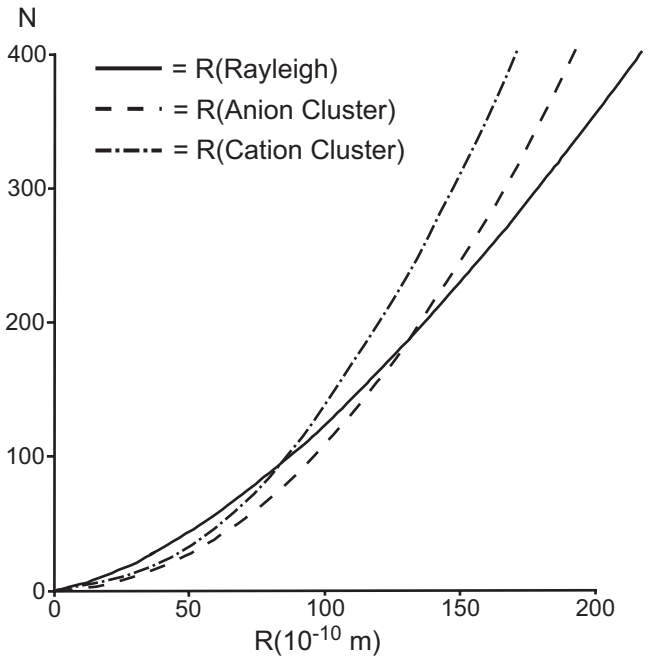

FIGURE 6. Predictions of the ion evaporation theory. The Rayleigh curve provides the droplet radius R and the number of elementary charges N of water droplets at the Rayleigh limit. The curves Cation Cluster and Anion Cluster show the threshold for ion evaporation at a given charge N and droplet radius R. For negatively charged droplets, ion evaporation is expected when $R = 140$ Å or smaller (1 nm = 10 Å) and for positively charged droplets at $R = 84$ Å. Below this radius ion evaporation replaces Coulomb fission. A radius of $R \approx 100$ Å or lower provides a benchmark for the region where ion evaporation takes over (after Thomson & Iribarne, 1979, see text).

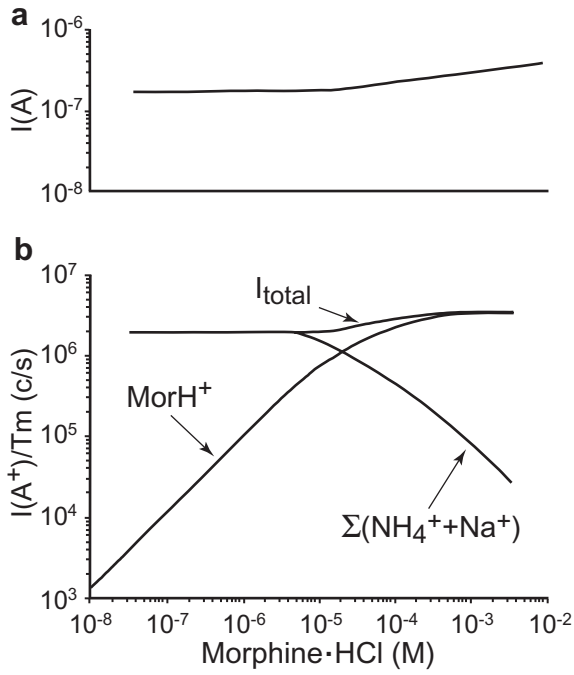

FIGURE 7. **a**: Electrospray current (amp) with increasing concentration of analyte MorphineHCl. Due to presence of impurity ions (Na^+ and NH_4^+) at a10^{-5} M level. I_{total} remains constant up to the point where the analyte $MorH^+$ reaches concentrations above 10^{-5} M. **b**: Analyte $MorH^+$ ion intensity (corrected for mass dependent ion transmission, Tm, of quadrupole mass spectrometer used) is proportional to concentration of MorphineHCL up to the point where the MorphineHCl concentration approaches concentration of impurity ions. (Reprinted from Kebarle & Tang, 1993, with permission from the American Chemical Society, copyright 1993.)

become part of the charge on the droplet surface and the ability to escape and enter the gas phase.
Two components;

$$\text{Two componenets}: \quad I_{A^+} = pf\frac{k_A C_A}{k_A C_A + k_E C_E} I \qquad (8a)$$

$$\text{Three components}: \quad I_{A^+} = pf\frac{k_A C_A}{k_A C_A + k_B C_B + k_E C_E} I \qquad (8b)$$

$$\text{For CA} \ll \text{CE}: \quad I_A = \text{const} \times C_A \quad \text{const} = \frac{k_A I_E}{k_E C_E} \qquad (8c)$$

Equation (8b) is for three components A^+, B^+, and E^+ with concentrations C_A, C_B, and C_E. In the regime where C_E is much larger than C_A, Equation (8a) reduces to Equation (8c). The experimental results (Kebarle & Tang, 1993) shown in Figure 7 give an example of a two-component system where the protonated morphine ion $MorH^+$ (analyte A) is used at varying concentration and the impurities NH_4^+ and Na^+ (contaminant electrolytes E) are present at constant concentrations. The observed linear dependence of the $MorH^+$ signal on morphine concentration in the log–log plot used has a slope of unity at low concentrations (10^{-8}–10^{-5} M) indicating that the $MorH^+$ ion is proportional to the morphine concentration. This region is suitable for quantitative determinations of analytes. At approximately 10^{-5} M the increase of the $MorH^+$ intensity with morphine concentration levels off because the $MorH^+$ concentration comes close to that of the contaminant E. Above that region $MorH^+$ Cl^- becomes the major electrolyte and the peak intensity of $MorH^+$ will grow only with the square root of the $MorH^+$ concentration.

Experiments with three components, two analytes (A and B) and the contaminant (E) lead to an unexpected result (see Fig. 8). In this experiment the concentrations of the two analytes, A = tetrabutylammonium and B = cocaine (upper figure) or B = codein (lower figure), were simultaneously increased such that $C_A = C_B$. The contaminant C_E remains constant. Equation (8) predicts that when C_A equals C_B and C_E is much larger, the relationship $I_A/I_B = k_A/k_B$ holds so that, on a log–log plot, the difference $\log I_A - \log I_B$ should correspond to the difference $\log k_A - \log k_B = \log(k_A/k_B)$, a constant and in general not equal to zero. However, this is not the case (see Fig. 8). The difference is constant only at high C_A ($=C_B$) concentrations and becomes zero at low concentrations.

The observed tendency of k_A/k_E to approach unity at low C_A, C_B indicates (Tang & Kebarle, 1993) that there is a depletion of the ion that has the higher sensitivity k. This is the

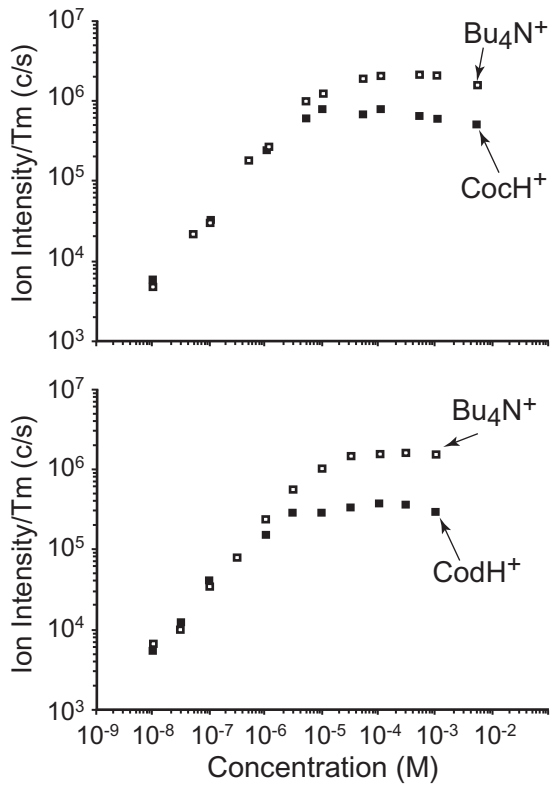

FIGURE 8. Ion intensities for pairs of analytes at equal concentration in solution. The different ESI sensitivities of the analytes are observable only at high analyte (above 10^{-5} M) concentrations. (Reprinted from Tang & Kebarle, 1993, with permission from the American Chemical Society, copyright 1993.)

tetrabutylammonium ion in the present example. This observation can be explained as follows. At $C_A = C_B \ll C_E \approx 10^{-5}$ M, the current I and the total charge Q of the droplets, and the number of charged droplets is determined by C_E. The ionic species A^+ and B^+ with large sensitivity coefficients (k_A, k_B) evaporate rapidly when reaching the droplet surface, resulting in a bulk depletion of A^+ and B^+. The ion A of higher sensitivity is depleted faster than B and the resulting lower concentration of A in the droplet, limits mass transfer to the surface and subsequent evaporation leading to an *apparent* $k_A = k_B$. These observations lead to the conclusion that determinations of the relative coefficients k_A/k_B should be performed only at high concentrations of C_A and C_B.

Experimental determination of the coefficient ratios k_A/k_B were performed (Tang & Kebarle, 1993) for a number of analytes in methanol by working at high concentrations C_A and C_B. It was found that the singly charged inorganic ions, Na^+, K^+, Rb^+, Cs^+, and NH_4^+ had low sensitivity coefficients, while surface active analyte ions which were expected to be enriched on the droplet surface had high coefficients that increased with the surface activity of the ions. Thus, assuming that $k^+_{Cs} = 1$, the relative values k_A for the ions were: $Cs^+ \approx 1$; $Et_4N^+ = 3$; $Pr_4N^+ = 5$; $Bu_4N^+ = 9$; $Pen_4N^+ = 16$; $HeptNH_3^+ = 8$, where Et, Pr, Bu, etc., stands for ethyl, *n*-propyl, *n*-butyl, etc. (see Table 1 in Tang & Kebarle, 1993). Tetraalkylammonium salts and alkylammonium salts, especially those with long chain alkyl groups, are known surfactants.

Assuming that IEM holds, ions at the droplet surface will leave the droplets and become gas-phase ions. In this case, the gas-phase ion sensitivity coefficient (k_A) for ions A^+ will depend on the relative surface population of the droplet surface, that is, on the surface activity of ions A^+ given by a surface activity equilibrium constant (K_{SA}), and also on the rate constant for ion evaporation. The rate constant for ion evaporation is also expected to increase with the surface activity of the ion, because surface active ions have low solvation energies (see Section IIH). In addition, ion evaporation will occur from first, second, or third generation progeny droplets (see Fig. 6). Because the progeny droplets have higher surface-to-volume ratios relative to the parent droplets, a large enrichment of the surface active ions is expected for the progeny droplets.

More recent work by Enke (1997) has led to some significant advances starting from somewhat different premises. Instead of working with the ion currents I, a conversion to mol/L charge was used. Thus the role of the ion current I was replaced with the molar concentration of the excess ionic charges $[Q]$. This can be done on the basis of the relationship (Eq. 9) given below:

$$[Q] = \frac{I}{F\Gamma} \tag{9}$$

where $[Q]$ is in mol/L electron charges, I is the total droplet current (TDC) in amps (coulomb/sec) measured with the TDC meter (see Fig. 1) F is Faraday's constant (96,485 coulomb/mol) and Γ is the flow rate through the spray capillary in L/sec.

The same type of relationship is also used in the conversion of the analyte currents I_A I_B, etc., into molar concentrations of charges on the droplets due to the given ion species. Thus, $[A^+]_S$ is the molar concentration of charges on the surface of droplets due to A^+ species, etc. The analyte A^+ was assumed to distribute itself between the interiors of the droplets with a concentration $[A^+]_I$ and as charge at the surface of the droplets $[A^+]_S$. It should be noted that while expressing $[A^+]_I$ in mol/L is straightforward, $[A^+]_S$ as mol/L at the surface is not because expressing the surface as volume is unconventional. However one could imagine that the ions (charges) at the surface are still interacting with a thin layer of solution below the surface and this corresponds to a volume.

An equilibrium between $[A^+]_S$ and $[A^+]_I$ was assumed. The other electrolytes were treated in the same way. Introduction of equations of charge balance and mass balance for each electrolyte led to an equation which predicts values for $[A^+]_S$, $[B^+]_S$, etc., on the basis of the parameters $[Q]$ which is known (see Eq. 9), the constants K_A, K_B, etc., and the concentrations C_A, C_B, etc.

Enke and Cech have made a number of important contributions to the mechanism and uses of electrospray that the interested reader will find very insightful and useful. For a representative sample, see Amad, Cech, and Enke (2000) and Cech and Enke (2000, 2001a,b).

In conclusion, quantitative determinations of the concentrations of ionic analytes in solution are possible but require special care. Quantitation of analytes that are not ionic in the solution but can be observed as ions via ESIMS can be expected

to be more difficult because ionization is possible only by proton transfer or ion-analyte adduct formation which probably occurs at or near the droplet surface.

J. Gas-Phase Ions of Macromolecules Such as Proteins and Protein Complexes Are Most Probably Produced by the Charged Residue Model (CRM)

Gas-phase ions of globular proteins and protein complexes are routinely produced by ESI. Native proteins are expected to remain folded when sprayed from a water–methanol solution that is close to a neutral pH. Folded (non-denatured) proteins lead to mass spectra consisting of a compact series of peaks that correspond to the molecular mass of the protein charged (in the positive ion mode) by a narrow range of numbers of H^+ ions. Thus a small protein like lysozyme in the molecular mass range of 15,000 Da is observed to lead to three peaks due to three different charge states with $Z = 8, 9, 10$. Obviously it is of special interest to understand why the proteins are multiply charged. Is the charge observed in the positive ion mode related to the charge in solution and determined by the number of basic residues that the protein has, or are there other factors involved such as a dependence on the ESI mechanism by which the protein is transferred from the solution to the gas phase?

An early study by R. D. Smith and co-workers (Winger et al., 1993) provided good evidence that protein ions are produced via CRM. This model assumes that the charged macro-ions are produced from very small droplets which contain one macromolecule. As this droplet evaporates completely the charges on the droplet are transferred to the macromolecule. If CRM holds, statistically one would also expect the observation of protein aggregates (multimers) as a result of more than one protein molecule being present in the final droplet. Winger et al. observed a preponderance of multiply charged monomers together with a series of dimers and trimers of decreasing low intensity; the charge to total mass ratio (z/m) value decreased with the degree of aggregate formation. Using a quadrupole mass spectrometer with a very high mass range, the authors were able to observe even higher multimers, and came to the conclusion that the results are consistent with CRM and a droplet evolution following a scheme of the type shown in Figure 6.

In later work, Smith and co-workers (Tolic et al., 1997) found an interesting empirical correlation between the molecular mass M and the average charge Z_{av} of ions formed from starburst dendrimers (see Eq. 10). Starburst dendrimers are multi-branched alkyl-amine polymers that have relatively rigid structures and are close to spherical, that is, with shapes resembling those of globular proteins.

$$Z^{obs} = aM^b \tag{10}$$

In Equation (10), Z_{obs} is the observed average charge state and M the molecular mass of the dendrimer, while a and b are constants. The value $b = 0.53$ led to the best fit. Standing and co-workers (Chernuschevich, 1998) obtained an identical relationship for a large number of non-denatured proteins, where the value of b was between $b = 0.52$ and 0.55.

Independently Fernandez de la Mora (2000) using the dendrimer data of Tolic et al., and including additional data from the literature for non-denatured proteins, was able to show not only that the empirical relationship (Eq. 10) holds, but also that the relationship can be derived on the basis of the Charged Residue Mechanism. The plot shown in Figure 9 is based on the data used by Fernandez de la Mora, but also includes the protein data of Chernuschevich (1998).

The derivation of Fernandez de la Mora was based on the following arguments. There was theoretical evidence that the evaporating charged droplets (which in the present context are assumed to contain one *globular* protein molecule) stay close to the Rayleigh limit. This assumption is supported by more recent experimental results (see Fig. 4a in Section IIF), which involve charged evaporating water droplets of 5–35 μm diameter. These show that the charge is approximately 95% of the Rayleigh limit when the droplets experience a Coulomb fission and approximately 75% of the Rayleigh limit immediately after the Coulomb fission. Thus, the droplets stay at all times close to the Rayleigh limit, within 95–75% of the limit. Fernandez de la Mora reasoned that the charged water droplet that contains a single protein molecule, in the final evaporation stage will transfer all charges to the protein. He assumed also that the protein will be neutral when all the water is gone so that the charges on the surface of the droplet become the charge of the protein observed in the ESI mass spectrum. While Fernandez de la Mora did not justify the assumption that the protein will be neutral when all the water is gone, evidence for the validity of this assumption is supplied in Section IIK where it is argued that ion pairing between positive and negative ions will occur as the solvent disappears. Such ion pairing will result in neutralization of the protein inside the vanishing droplet.

The radius R of the protein can be evaluated with Equation (11), where φ is the density of the protein, $N_A = 6 \times 10^{23}$ the Avogadro Constant (molecules per mole), R the radius of the protein, and M the molecular mass of the protein.

$$\frac{4}{3\pi R^3 \varphi} N_A = M \tag{11}$$

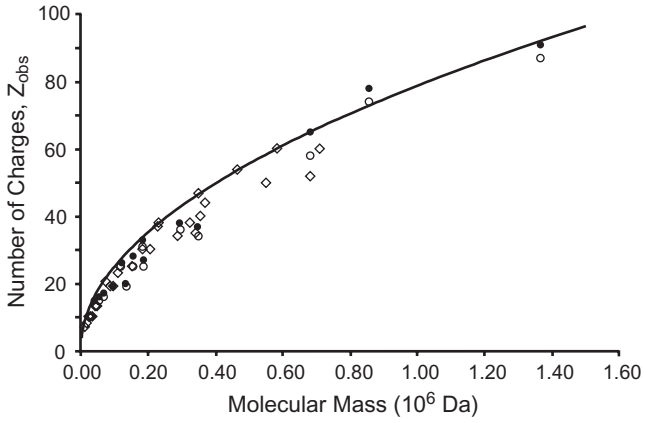

FIGURE 9. Reproduction of a plot used by Fernandez de la Mora (2000) extended to include data from Chernuschevich (1998). Z_{obs} are the number of charges of proteins produced by ESIMS under non-denaturing conditions. Fernandez de la Mora: ● highest charge, ○ lowest charge. Chernuschevich: ◇ average charge. Solid curve corresponds to charge predicted by Equation (12).

Fernandez de la Mora assumed that non-denatured proteins have the same density φ as water, $\varphi = 1\ \mathrm{g/cm^3}$. Evidence in support of that assumption is based on mobility measurements by Jarrold and Clemmer (Shelimov et al., 1997) and can be found in section 2.2 of Fernandez de la Mora (2000). The number of charges Z on the protein is taken to be the same as the number of charges on a water droplet of the same radius R that just contains the protein and is at the Rayleigh limit. The number of charges Z can be obtained by expressing the charge, $Q = Z \times e$ and substituting it in the Rayleigh equation (Eq. 6) using the relationship between the molecular mass M and the radius of the droplet: $M = 4/3\pi R^3 \varphi N_A$. The result is given in Equations (12a) and (12b), where Z is the number of charges of the protein, γ the surface tension of water, ε_o the electrical permittivity, e the electron charge, N_A the Avogadro Constant, φ the density of water, and M the molecular mass of the protein. Using a constant 0.078 in Equation (12b) allows the calculation of the number of charges on a protein of molecular mass M (in mega-Daltons).

$$Z = 4\left(\frac{\pi\gamma\varepsilon_0}{e^2 N_A \varphi}\right)^{1/2} \times M^{1/2} \qquad (12a)$$

$$Z = 0.078 \times M^{1/2} \qquad (12b)$$

The solid curve in Figure 9 gives the predicted charge based on Equation (12a). Good agreement with the experimental results is observed. Notable also is the predicted exponent of M which is 0.5, while the exponent deduced from the experimental data of Figure 9 is 0.53. The agreement of Equation (12) with the observed charges Z can be considered as very strong evidence that globular proteins and protein complexes are produced by CRM.

Most of the data points in Figure 9 were obtained not with neat water as solvent, but from solutions of water and methanol. These solutions are easier to use in ESIMS because neat water, due to its high surface tension, can initiate electrical gas discharges at the spray needle (see Section IID). Nevertheless, the surface tension of water ($\gamma = 73 \times 10^{-3}$ (N/m); see Table 1) was used by Fernandez de la Mora in Equation (11) for the surface tension of the droplets. The surface tension of methanol $\gamma = 22.6 \times 10^{-3}$ (N/m) is much smaller. However, it is expected that the evaporating droplets will lose methanol preferentially because of the much higher vapor pressure of methanol. Therefore the final droplets that contain the protein will be very close to neat water droplets. This can be expected because there has been an extremely large loss of solvent by evaporation before the final very small droplets containing the protein are formed (see Fig. 6 and associated discussion). A recent compilation of data by Heck and co-workers (Heck & van den Heuvel, 2004) has shown that the square root dependence of the charge Z on M (see Eq. 11a) also holds for protein complexes.

The experimental points in Figure 9 show a considerable scatter and deviations from the theoretical curve. However, this is most likely due to the measurements being made in different laboratories using different instruments. Recent work by Kaltashov and Mohimen (2005) (Fig. 10), where all the experimental points were obtained using the same mass spectrometer, provide a very good fit. However, one point in Figure 10 shows a considerable deviation for a protein far from spherical, that is, outside the original assumptions used by

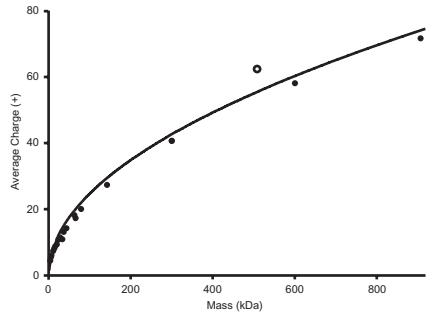

FIGURE 10. Plot of average charge of proteins observed by Kaltashov and Mohimen (2005) versus molecular mass of protein. The solid line curve gives average charge predicted by the Fernandez de la Mora equation (Eq. 12). A very good fit is observed except for one protein which has a significantly higher charge Z. This protein is ferritin, with a mass $\approx$510 kDa. Ferritin is close to spherical but has a cavity that increases its surface. (The graph was graciously provided to the authors by Dr. Justin Benesh.)

Fernandeze de la Mora in deriving Equation (12). In this rare case the charge is determined by the surface area of the protein determined using crystallographic data, limiting the practical usefulness.

Fernandez de la Mora did not consider the actual chemical reactions by which the charging of the protein occurs. These reactions will depend on which additives were present in the solution. Thus, in the presence of 1% of acetic acid in the solution, the charges at the surface of the droplets will be H_3O^+ ions. Charging of the protein will occur by proton transfer from H_3O^+ to functional groups on the surface of the protein that have a higher gas-phase basicity than H_2O. The *gas-phase* basicities are relevant because the solvent will essentially have disappeared. There are plenty of functional groups on the protein that have gas-phase basicities that are higher than that of H_2O. These could be basic residues or amide groups of the peptide backbone at the surface of the protein. Gas-phase basicities of several representative compounds are given in Table 4 (Section IIM).

While Fernandez de la Mora's CRM has received wide acceptance, more recent work by Samalnikova and Grandori (2003, 2005) questioned the validity of the model. However, the conclusions of Samalnikova and Grandori were questioned by Nesatty and Suter (2004).

In summary, the Charged Residue Mechanism has allowed quantitative predictions of the protein charge state in the gas phase using a simple correlation between charge state and protein mass and is well supported for proteins of widely varying mass. Proteins with large deviations from the spherical shape have a charge higher than that predicted by Equation (12). This is not in direct contradiction of CRM because larger precursor droplets are required for non-spherical proteins and these larger droplets will have higher charges.

Very recent work by Michael Gross and co-workers (Hogan et al., 2008) proposes a modification of CRM in which CRM is preceded by IEM. This mechanism is expected (Hogan et al., 2008) when salt additives (buffers) such as ammonium acetate or triethylacetate are present in millimolar concentrations in the

solution that is electrosprayed. The charged states of native proteins observed is lower when the ammonium buffer is used and much lower when the triethylammonium is used, when compared with the charged states observed in the absence of these buffers. The authors propose that the lower charge states are due to an ion evaporation stage (IEM) that precedes the charged residue formation (CRM) of the protein. IEM is expected to be much more facile with triethylammonium ions because these surface active ions will require much lower energy to escape from the charged droplet surface. Thus as all solvent evaporates from the droplet fewer charges will be left for the protein.

K. Some Features Observed in Mass Spectra of Proteins That Are Due to the ESI or Nano-ESI Mechanism

1. Effects of Salt Additives on Mass Spectra of Proteins. Ion Pairing Reactions with Proteins Due to Salt Additives in Solution

The extensive evaporation of solvent in the stages preceding the formation of the gas phase analyte (see Sections IIF and IIG) leads to a very large increase of the concentration of solutes present in the solution. This is particularly the case for native (folded) proteins which are produced by the Charged Residue Mechanism. In the presence of salt additives in millimolar initial concentrations, the concentration increase will lead to ion pairing of positive with negative ions. These ion pairing reactions will also combine solute ions with ionized residues of the protein that happen to be at or near the surface of the protein. This pairing can start long before all the solvent has evaporated. As will be seen later, the occurrence of pairing is not always evident in the observed mass spectra. An important example of such an ion pairing additive is ammonium acetate.

On complete evaporation of the droplet, charges at the surface of the droplet will lead to charging of the protein. The presence of a salt additive in the solution will lead to many if not all charges being due to the positive ions supplied by the additive; the additive ions charge the protein.

The above phenomena are clearly observed in the mass spectrum when metal salts are deliberately added. The spectrum of folded ubiquitin, obtained with nanospray using an aqueous solution containing 25 μM ubiquitin and 1 mM NaI, is shown in Figure 11. The $Z = +6$ charge state is shown. This is by far the most abundant charge state observed with ubiquitin (Verkerk & Kebarle, 2005). A series of groups of peaks containing Na^+ and NaI is observed and the composition of these ions is given in the figure caption. The observed ions can be rationalized by the operation of two processes: (a) replacement of the H^+ charges with Na^+ charges where the Na^+ come from the surface of the droplets such that the ultimate state is due to replacement of all the H^+ with Na^+. (b) Ion pairing of Na^+ ions in the solution of the droplet with ionized acidic residues on the surface of the protein and ion pairing of I^- with ionized basic residues at the surface of the protein.

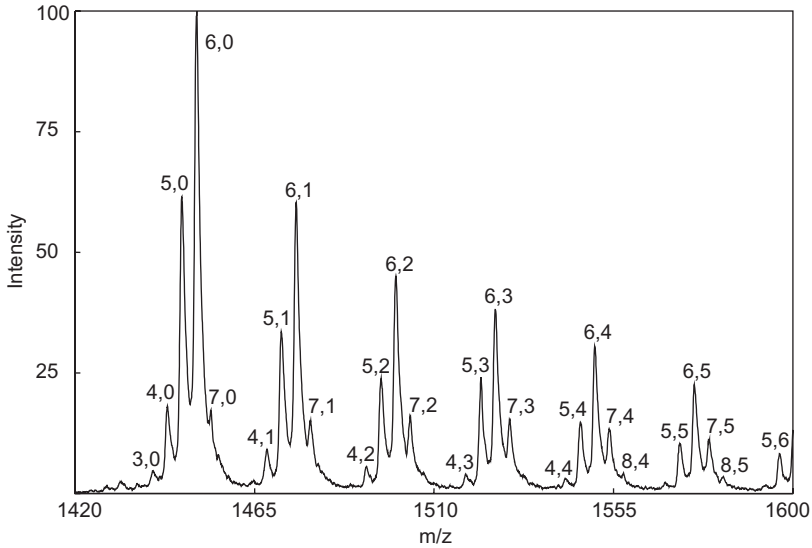

FIGURE 11. Mass spectrum of the major $Z = +6$, charge state of Ubiquitin obtained with an aqueous solution of 25 μM Ubiquitin containing 1 mM NaI. In the absence of NaI essentially only one peak is observed corresponding (ubiquitin) + $6H^+$. The observed first group of peaks corresponds to Ubiquitin where the H^+ charges are gradually replaced with Na^+. The largest peak in the first group, labeled 6.0 corresponds to ubiquitin + $6Na^+$. The second group has the same composition as the first group but each ion contains also one Na^+ and one I^-. The next group contains two Na^+ and two I^- and so on. The number n, of Na^+ ions is indicated with the first number over the peak, while the number m of Na^+I^- is given by the second number. (Reprinted from Verkerk & Kebarle, 2005, with permission from Elsevier, copyright 2005.)

The spectrum (Fig. 11) was obtained (Verkerk & Kebarle, 2005) at a low ratio of nozzle (spray capillary) to skimmer potential, so that there was little collisional activation (CAD) of the protein. At a high CAD, multiple losses of HI were observed (see Fig. 12). All the peaks that contained $Na^+ + I^-$ ions have disappeared and are replaced by peaks due to Na^+ adducts.

The observations based on Figures 11 and 12 can be easily explained using *gas-phase* chemistry:

(a) Charging reactions by Na^+. The sodium ion goes either on ionized acidic residues (ion pairing) or on the amide groups of the protein back bone. The Na^+ bonding is expected to be extremely strong at the ion pairing sites and strong at the amide site (see Table 3) and therefore no loss of Na is expected even at high CAD conditions.

(b) Ion pairing reactions involving Na^+ going to the same sites as in (a) and I^- going predominantly to the ionized basic residues. No net charging occurs. At high CAD conditions HI is formed by reaction (13) where the reacting basic residue shown is lysine:

$$\begin{aligned} &\text{Protein} - (CH_2)_4 - NH_3^+ - I^- \\ &= \text{Protein} - (CH_2)_4 - NH_2 + HI \end{aligned} \qquad (13)$$

Experiments involving the salts NaCl and NaAc, where Ac denotes the acetate anion, showed (Verkerk & Kebarle, 2005) that the energy required for the HX dissociation decreased in the order HI, HCl, HAc. It was also shown that this order is expected on the basis of theoretical calculations, and that the energy required is well within the range provided by the CAD used.

Additional evidence that the basic side chains are involved in the dissociation reaction was obtained by experiments where much higher concentrations of sodium acetate were added so as to be certain that all the ionized acidic sites were paired with Na^+ and all basic sites with the acetate anions. The mass spectrum of the $Z = 6$ charge state for ubiquitin and sodium acetate at high CAD is shown in Figure 13. The sharp break of peak intensity past $n = 18$ shows that the observed ubiquitin ion has 6 Na^+ charges and 12 ionized acidic sites paired to Na^+ ions giving a total of $n = 18$. The acetate anions that had ion paired with the ionized (protonated) basic sites have fallen off as acetic acid by pulling of a proton from the ionized site. Thus, the experiment predicts that ubiquitin had a total of 12 acidic sites that are at or near the surface of the protein. This is exactly the number expected from the known structure of ubiquitin. This result provides strong evidence for the proposed ion pairing mechanism (Verkerk & Kebarle, 2005).

2. Why Is Ammonium Acetate Such a Popular Salt Additive to Solutions Used for ESIMS?

Ammonium acetate at millimolar concentrations is often used as an additive to solutions, particularly so when the analytes are proteins. It acts as a buffer, even though a very weak one, and the assumption generally is made that this buffer action is the cause for its popularity. But ammonium acetate has another most useful property which was not recognized. It leads to very clean mass spectra of the multiply protonated proteins.

Sodium ions are a very common contaminant in protein samples. This is a consequence of the ''salting-out'' precipitation procedure used in the isolation of proteins. Even though the sodium impurity concentrations in the sprayed solution can be low, sodium adducts to the protein result in a mass shift that can cause difficulties in the interpretation of the mass spectrum. Use of ammonium acetate prevents the formation of sodium adducts

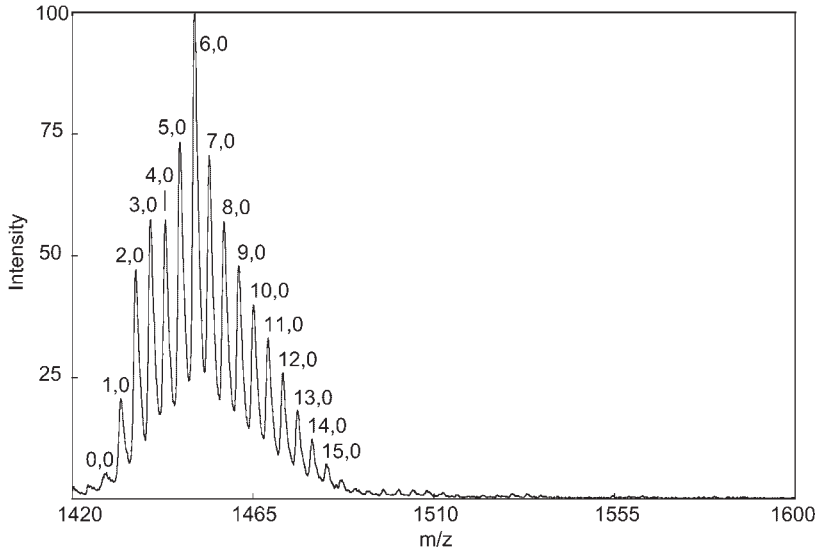

FIGURE 12. Mass spectrum of ubiquitin $Z = 6$ charge state under the same conditions as in Figure 11 but with high collisional activation (CAD). All the peaks that contained Na^+I^- pairs have disappeared and are replaced by uncharged Na adducts. This observation is consistent with loss of HI where the I^- ions, paired to an ionized basic residue, dissociated as HI. (Reprinted from Verkerk & Kebarle, 2005, with permission from Elsevier, copyright 2005.)

TABLE 3. Bond energies, , for reaction: $M^+B = M^+ + B$ in the gas phase

M^+	B						
	H_2O	NH_3	*i*-PrOH	Acetamide	N-methyl acetamide	Serine	Proline
Na^+	22.1[c]	25.6[c]	27.0[e]	35.6[c]	38.0[d]	45.0[c]	44.2[c]
K^+	16.9[b]	17.8[b]	--	--	--	--	--

[a]All values in kmol/mol at 298 K. For additional data on Na^+B, and K^+B complexes, see http://webbook.nist.gov/.

[b]Davidson and Kebarle (1979).
[c]Hoyau et al. (1999).
[d]Klassen et al. (1996).
[e]Armentrout and Rodgers (2000).

to the protein. The results described in the preceding part (11a) provide the mechanism by which this occurs. The ion pairing reactions in the presence of ammonium acetate are shown in Equation (14).

$$^+H_3N(CH_2)_2 - \text{Prot} - (CH_2)2COO^- + NH_4^+ + CH_3COO^- = CH_3COO^-H_3N^+(CH_2)_2 - \text{Prot} - (CH_2)2COO^-NH_4^+ \quad (14)$$

For simplicity, the equation shows only one ionized basic and acidic residue of the protein. The much larger concentration of the ammonium acetate relative to the sodium ion impurity leads to ion pairing that involves only acetate and ammonium ions. Subjecting the resulting protein to collisional activation in the gas phase leads to facile loss of acetic acid and ammonia as shown in Equation (15).

$$CH_3COO^-H_3N^+(CH_2)_2 - \text{Prot} - (CH_2)2COO^-NH_4^+ \rightarrow CH_3COOH + H_2N(CH_2)_2 - \text{Prot} - (CH_2)_2COOH + NH_3 \quad (15)$$

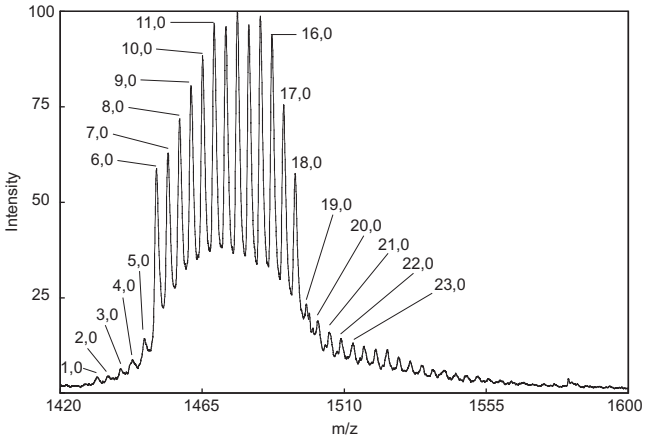

FIGURE 13. Mass spectrum showing $Z = 6$ charge state obtained with ubiquitin 25 μM, and a very high, 5 mM, concentration of sodium acetate. Observed at high CAD where all acetate anions have fallen off as acetic acid molecules. The sharp break of peak intensity past $n = 18$, marks that the observed ubiquitin has 6 Na^+ charges and 12 sodiated acidic sites on the protein. (Reprinted from Verkerk & Kebarle, 2005, with permission from Elsevier, copyright 2005.)

The dissociation is facile because the bond energy for the dissociation is only 15 kcal/mol for acetic acid and 11 kcal/mol for ammonia (Verkerk & Kebarle, 2005). The net effect of the complete process (Eqs. 14 and 15) is equivalent to a proton transfer from the ionized basic site to the ionized acidic site. Thus the molecular weight of the protein was not changed but the positive and negative groups were neutralized. Thus a clean mass spectrum of the protein is obtained without a mass change.

Negative ion impurities due to anions of strong acids, such as the phosphate or trifluoroacetate anions, result in strongly bonded adducts to the ionized basic residues. This can be prevented by using ammonium acetate as a source for obtaining a much higher concentration of the acetate ion. An important example is the use of trifluoroacetic acid (TFA) in the mobile phase in liquid chromatography-mass spectrometry. The presence of the TFA anion in the eluent leads to ion suppression and corresponding loss of sensitivity in ESIMS; addition of ammonium acetate to the solution removes this loss (Shou & Naidong, 2005).

L. Determinations of Equilibrium Constants of Association Reactions in Solution and Possible Sources of Error Due to the ESI Process

The determinations of equilibrium constants in solution by ESIMS can be divided into two categories: (a) equilibria involving small reactant ions and ligands. Readers interested in equilibria among small reactants can find useful literature information in the recent work by Zenobi and co-workers (Wortman et al., 2007). (b) Equilibria involving macro-ions such as proteins with ligands which may be large organic molecules. In both cases application of ESIMS can lead to erroneous results. The determination of the association constants of protein–substrate complexes via nanospray is widely used. Therefore, only the protein work will be considered here.

The formation of non-covalently bonded complexes of proteins with substrates is an extremely important class of reactions in biochemistry (Heck & van den Heuvel, 2004). It involves processes such as enzyme–substrate interactions, receptor–ligand binding, assembly of transcription complexes, and so on. The determination of these constants in solution has been an important component of biochemistry for many years. The major advantages of ESI over the established methods are the much smaller quantity of analyte required and the ability to identify complexes involving multiple components. The first

ESIMS study of non-covalent complexes involving proteins, by Ganem, Li, and Henion (1991), was followed by a large number of studies (Loo, 1997; Ayed et al., 1998; Daniel et al., 2002). However the method is still in a state of development and improvement. A brief description of the method and recent developments are given below.

Consider the general reaction (Eq. 16a) where P is the protein, S is the substrate (ligand), and the reaction has reached equilibrium. The equilibrium constant K_{AS} for the association reaction (Eq. 16a) is given by Equation (16b) where [P], [S], and [PS] are the concentrations at equilibrium.

$$P + S = PS \tag{16a}$$

$$K_{AS} = \frac{PS}{P \times S} = \frac{I_{PS}}{I_P \times I_S} \tag{16b}$$

Sampling the solution via ESI, the concentrations are often replaced with the ESIMS observed peak intensities, I_P, I_S, and I_{PS}.

One can repeat the experiment at several gradually increasing concentrations of S, and examine whether the association constant, evaluated with Equation (16b), remains constant. ESIMS determinations of $I_{PS}/I_P \times I_S$ with this ''titration'' method have been often in agreement with the requirements of Equation (16b) and have also provided K_{AS} values in agreement with data in the literature obtained by conventional methods (Loo, 1997; Ayed et al., 1998; Daniel et al., 2003). When the molecular mass of S is much smaller than those of P and PS, as is often the case, erroneous results may be obtained due to mass-dependent transmission of the MS analyzer. Therefore, it is advantageous to use only the ratio of I_{PS}/I_P, because P and PS have a similar mass. Zenobi and co-workers have provided an equation for the determination of K_{AS} with the titration method in which I_S is eliminated.

From the standpoint of the mechanism of ESI, the agreement of the K_{AS} values determined via ESIMS with values obtained with other methods appears surprising. One could expect that the very large increase of the concentration of the solutes in the charged droplets due to solvent evaporation will lead to an apparent K_{AS} that is much too high. However, the equilibrium shift need not occur if the rates of the forward and reverse reactions leading to the equilibrium are slow compared to the time of droplet evaporation.

Peschke, Verkerk, and Kebarle (2004) using experimental information of Smith, Flagan, and Beauchamp (2002) on the evaporation of charged water droplets produced by ESI and their fissions, evaluated an approximate droplet history scheme for water droplets produced by nanospray. The early part of this scheme is shown in Figure 5. Because the initial droplets produced by nanospray are very small, their evaporation is very fast so that they reach the Rayleigh instability condition in just several μsec (see Fig. 5). It could be established (Peschke, Verkerk, & Kebarle, 2004) that the first generation progeny droplets will be the major source of analyte ions. Assuming even the fastest possible reaction rates, that is, diffusion limit rates in water for the forward reaction $P + S \rightarrow PS$, it could be shown that the time is too short for the equilibrium (Eq. 16) to shift in response to the increasing concentration due to solvent evaporation. Because the proteins are very large, the diffusion limit depends on the diffusion of the substrate S, that is, the rate constant at the diffusion limit decreases with an increase of the size of S. Substrates of medium size such as erythrohydroxy aspartate, adenosine-diphosphate and -triphosphate, with diffusion limited rate constants $k = 10^6 - 10^7\ M^{-1}\ sec^{-1}$, are too slow to cause an equilibrium shift that will lead to a significant error in the K_{AS} determination. Thus, at least for nanospray, an equilibrium shift for substrates that are not too small is not expected.

Because proteins are most probably transferred to the gas phase via CRM, another question must be examined also. Assuming that close to equal concentrations of the protein and substrate, in the 10 μM range, were used, the evaluation (Peschke, Verkerk, & Kebarle, 2004), shows that in most cases there will be one protein and one substrate molecule in the average first generation progeny droplet that is in the process of evaporating down to the size of the protein. In that case, the P and S will form a *non-specific* complex because the substrate S makes a random encounter with the protein and has ''no time'' to find the site required for *specific* strong bonding. Since the mass of the non-specific complex is the same as that of the specific complex, the observed peak intensity I_{SP} will lead to an apparent K_{AS} that is too high. But this need not be the case. The weakly bonded non-specific complexes are expected to fall apart easily in the clean up stages of the interface to the mass analysis region, thereby minimizing the non-specific contribution in the measured K_{AS} (Peschke, Verkerk, & Kebarle, 2004).

The above *a priori* assumption about non-specific complexes, while logical, may not predict the correct outcome in all cases. It neglects to consider the strong ion-neutral bonding in the gas phase discussed in Section IIM and Table 3, and the fact that the protein will be multiply charged as the charged droplet dries out. Strong hydrogen bonds can form between charged (protonated) sites of the protein and functional groups of the substrate such as $-OH$ and $-NH_2$ groups. A recent study by Wang, Kitova, and Klassen (2003) described exactly such effects for protein–carbohydrate protein–substrate complexes. Not only did they observe PS and SPS complexes in the gas phase, but the non-specific bond was found to be stronger than the specific bond! This suggested that the non-specific S–P bond was to a protonated site of the charged protein. The bond energies were determined with the Blackbody Infrared Radiative Dissociation (BIRD) technique using a modified Fourier Transfer Ion Cyclotron (FTICR) mass spectrometer. Later work from this group (Sun et al., 2006) describes methods with which corrections can be made for the presence of non-specific protein substrate complexes which form in the evaporating droplets that are the precursors of the gas phase protein ions.

Another source of error due to the decomposition of a *specific* complex (trypsin–benzamidine), in the transfer of the complex to the mass spectrometer, was recently reported (Sun, Kitova, & Klassen, 2007). It was found that the decomposition was much reduced by using additives such as imidazole in the solution. It was suggested that the stabilizing effect may be due to formation in solution of imidazole adducts to the trypsin–benzamidine complex. The dissociation of these adducts in the clean up stage leading to the mass analysis region provides a cooling effect and thus protects the trypsin–benzamidine complex.

M. Two Different Worlds: Ionic Reactions in Solution and in the Gas Phase

In ESIMS the analytes experience both solution and gas-phase conditions and the observed mass spectrum therefore can reflect *both* solution and gas phase conditions. Many practitioners of ESIMS with a biochemical background are well acquainted with non-covalent and ionic reactions in aqueous solution, but lack a strong background in gas-phase interactions. This section provides a brief overview of interactions in the liquid and gas phases.

In water the separation of an ion pair such as Na^+Cl^- is spontaneous, but in the gas phase the separation requires the very large energy input of 148 kcal/mol (NIST database: http://webbook.nist.gov/), a value much larger than the energy required to break a C–C or a C–H covalent bond.

$$NaCl_{(g)} = Na^+_{(g)} + Cl^-_{(g)} \quad \Delta E \approx 148\,\text{kcal/mol} \tag{17}$$

A salt like NaCl is soluble in water because of the strong solvation interactions of the Na^+ and Cl^- with the water molecules. Non-polar compounds like the hydrocarbons are weakly soluble in water because water molecules interact strongly with each other via their high polarity and by forming hydrogen bonds, thus excluding the hydrocarbon molecules (Kauzmann, 1959). The hydrocarbon molecules have weak van der Waals interactions with water molecules and somewhat stronger van der Waals interactions with each other. At low concentrations of the hydrocarbon in water, this leads to formation of hydrocarbon islets in the water medium. Higher hydrocarbon concentrations lead to the familiar formation of two separate liquid phases.

Unfolded (i.e., denatured) proteins have regions that are hydrophobic and other regions which are strongly hydrophilic as a result of ionized residues. The denatured protein will tend to fold spontaneously, such that the ionic residues face and interact with the water molecules while the hydrophobic sections point inward and interact with each other.

When charged analytes such as proteins are present in the evaporating droplets, ions such as Na^+ (due to salt impurities) will begin to ion pair with the ionized acidic residues of the protein. This ion pairing will be driven by the very large loss of solvent by evaporation from the droplets. In the absence of solvent the bonding of these ion pairs is so strong that no amount of collision energy provided in the clean up stages of the interface leading to the mass analysis region can remove the undesired Na^+ adducts. Examples of such ion pairing effects were given in Section IIK.

In the gas-phase positive ions such as Na^+ and K^+ form fairly strongly bonded adducts with polar as well as aromatic compounds B. The bond dissociation energies corresponding to the reaction:

$$M^+B = M^+ + B \tag{18}$$

for a number of such ion–ligand complexes are given in Table 3.

Of special interest are ligands that model functional groups of proteins. For example, *N*-methylacetamide, which models the amide groups $-CH_2CONH-CH_2-$ of the protein backbone, forms a bond with Na^+ with a bond dissociation energy of that is equal to 36 kcal/mol. Comparing this with the value for acetone which is 30 kcal/mol (Hoyau et al., 1999; McMahon & Ohanessian, 2000), the stronger interaction with the methylacetamide must be due to a contribution of the $-NH_2-$ group. For the amino acids serine and proline, the binding energy (~45 kcal/mol) is even higher, probably due to participation of neighboring groups. These high values indicate that Na^+ adducts to the amide groups of the proteins also will not dissociate in the clean up stages of the ESI mass spectrometer.

The charging of an analyte such as a protein in the vanishing droplets will, as discussed in previous sections, involve the excess charges at the droplet surface. Using an acidic additive, like acetic or formic acid, will result in charging of the protein by proton transfer from H_3O^+ to basic residues and the amide groups of the protein.

The gas-phase basicities of the solvent molecules (H_2O in the present case) and of compounds modeling functional groups of the protein are expected to determine the outcome of the proton transfer reaction. Table 4 provides gas-phase basicity data for several representative compounds that model protein functional groups (gas-phase basicity data for thousands of compounds are available on the NIST database freely available at http://webbook.nist.gov/). The reaction rate constants of proton- or ligand-transfer reactions that form the vast majority of ion molecule reactions in the gas phase can be predicted on the basis of the thermochemistry of the gas phase reactions. Thus, for example, the proton transfer reaction: $AH^+ + B \rightarrow A + BH^+$ will proceed at collision rates, that is, without activation energy when the gas-phase basicity $GB(B) > GB(A)$. The absence of activation energy is due to the attraction between the charge of the ion and the polarizable molecule. This attraction leads to a ''collision'' where the ion and molecule spiral around their center-of-mass until they collide with each other. These spiraling collisions lead to rate constants that are very large. Furthermore, the energy released by the ''collision'' is generally sufficient to

TABLE 4. Some gas-phase basicities of bases B for reaction: $BH^+ = B + H^+$

Base	GB(B)[a] (kcal/mol)	Base	GB(B)[a] (kcal/mol)
H_2O	157.7	NH_3	195.7
$(H_2O)_2$	181.2	CH_3NH_2	206.6
CH_3OH	173.2	$C_2H_5NH_2$	210.0
$(CH_3OH)_2$	196.3	$(CH_3)_2NH$	214.3
C_2H_5OH	178.0	$(CH_3)_3N$	219.5
$(CH_3)_2O$	179.0	*N*-methyl acetamide	205.0
$(C_2H_5)_2O$	182.7	Pyridine	214.8

[a]GB(B) = gas-phase basicity; GB(B)[a] = . All values from NIST database.

activate the reaction. For experimental and theoretical evidence, see Stevenson and Schissler (1958) and references therein. Stevenson and co-workers were prominent early contributors to the development of the field of ion–molecule reactions in the gas phase.

Proteins in general will be easily protonated because they have basic residues with relatively high GBs. Thus GB(lysine) modeled by GB(*n*-propyl amine) = 212 kcal/mol (Table 4) has a much higher GB than GB($(H_2O)_2$) = 181 kcal/mol, so a proton transfer to lysine is expected. Proton transfer to the backbone amide group modeled by GB(*N*-methylacetamide) = 205 kcal/mol is also expected. In these statements we have assumed that the proton donors in the proton transfer are $(H_2OHOH_2)^+$ species at the surface of the droplet. This is a plausible assumption particularly if the CRM holds.

On the other hand, protonation of a sugar like glucose is unlikely because the GB(glucose), roughly modeled by GB(ethanol) = 178 kcal/mol (Table 4), is too low to allow proton transfer from $(H_2OHOH_2)^+$. Experimentally it was observed that good ESI mass spectra of carbohydrates cannot be obtained by protonation (Reinhold, Reinhold, & Castello, 1995). However, spectra could be obtained by sodiation through the addition of mM concentrations of sodium acetate to the carbohydrate solution (Reinhold, Reinhold, & Castello, 1995). The gas phase sodium ion affinities for sugars and even monosaccharides such as glucose do not seem to have been determined. However, high sodium affinities are expected because hydroxy groups on adjacent carbon atoms are present which will lead to bidentate interactions with the sodium ion.

REFERENCES

Amad MH, Cech NB, Enke CG. 2000. Importance of gas phase proton affinities in determining the electrospray ionization response for analytes and solvents. J Mass Spectrom 35:784–789.

Armentrout PB, Rodgers MT. 2000. An absolute sodium cation affinity scale: Threshold collision induced dissociation energies and ab initio theory. J Phys Chem A 104:2238–2244.

Ayed A, Krutchinsky AN, Ens W, Standing KG, Duckworth HW. 1998. Qualitative evaluation of protein-protein and ligand-protein equilibria of a large allosteric enzyme by electrospray ionization time of flight mass spectrometry. Rapid Commun Mass Spectrom 12:339–344.

Blades AT, Ikonomou MG, Kebarle P. 1991. Mechanism of electrospray mass spectrometry. Electrospray as an electrolysis cell. Anal Chem 63:2109–2114.

Cech NB, Enke CG. 2000. Relating electrospray response to nonpolar character of small peptides. Anal Chem 72:2717–2723.

Cech NB, Enke CG. 2001a. Practical implications of some recent studies in electrospray ionization fundamentals. Mass Spectrom Rev 20:362–387.

Cech NB, Enke CG. 2001b. Effect of affinity for droplet surfaces on the fraction of analyte molecules charged during electrospray droplet fission. Anal Chem 73:4632–4639.

Chernuschevich IV, Ens W, Standing KG, editors. 1998. New methods for the study of biomolecular complexes. Dordrecht, Boston, London: Kluwer Academic Publishers. p 101.

Chernushevich IV, Bahr U, Karas M. 2004. Nanospray ''Taxation'' and how to avoid it. Rapid Commun Mass Spectrom 18:2479–2485.

Cloupeau M, Prunet-Foch B. 1994. Electrohydrodynamic spraying functioning modes: A critical review. J Aerosol Sci 25:1021–1036.

Cloupeau M. 1994. Recipes for use of EHD spraying in cone-jet mode and notes on corona discharge. J Aerosol Sci 25:1143–1157.

Daniel JM, Friess SD, Rajagopalan S, Wend S, Zenobi R. 2002. Quantitative determination of noncovalent binding interactions using soft ionization mass spectrometry. Int J Mass Spectrom 216:1–27.

Daniel JM, McCombie G, Wend S, Zenobi R. 2003. Mass spectrometric determination of association constants of adenylate kinase with two noncovalent inhibitors. J Am Soc Mass Spectrom 14:442–448.

Davidson WR, Kebarle P. 1979. Binding energies and stabilities of potassium ion complexes from studies of the gas phase ion equilibria: $K^+ + M = K^+M$. J Am Chem Soc 98:6133–6138.

di Lena F, Quintanilla E, Chen P. 2005. Measuring rate constants for active species in the polymerization of ethylene by MAO-activated metallocene catalysts by electrospray ionization mass spectrometry. Chem Commun 46:5757–5759.

Dole M, Mack LL, Hines RL, Mobley RC, Ferguson LD, Alice MB. 1968. Molecular beams of macroions. J Chem Phys 49:2240–2249.

Enke CG. 1997. A predictive model for matrix and analyte effects in the electrospray ionization of singly-charged ionic analytes. Anal Chem 69:4885–4893.

Fernandez de la Mora J, Locertales IG. 1994. The current emitted by highly conducting Taylor cones. J Fluid Dyn 260:155–184.

Fernandez de la Mora J. 2000. Electrospray ionization of large multiply charged species proceeds via Dole's charged residue mechanism. Anal Chim Acta 406:93–104.

Fernandez de la Mora J. 2007. The fluid dynamics of Taylor cones. J Annu Rev Fluid Mech 39:217–243.

Gamero-Castano M, Fernadez de la Mora J. 2000a. Kinetics of small ion evaporation from the charge and mass distribution of multiply charged clusters in electrosprays. J Mass Spectrom 35:790–803.

Gamero-Castano M, Fernadez de la Mora J. 2000b. Direct measurement of ion evaporation kinetics from electrified liquid surfaces. J Chem Phys 113:815–832.

Ganem B, Li Y, Henion JD. 1991. Detection of non-convalent acceptor-ligand complexes by mass spectrometry. J Am Chem Soc 113:6294–6296.

Gomez A, Tang K. 1994. Charge and fission of droplets in electrostatic sprays. Phys Fluids 6:404–414.

Grimm RL, Beauchamp JL. 2002. Evaporation and discharge dynamics of highly charged droplets of heptane, octane and p-xylene generated by electrospray ionization. Anal Chem 74:6291–6297.

Heck AJR, van den Heuvel RHH. 2004. Investigation of intact protein complexes by mass spectrometry. Mass Spectrom Rev 23:368–389.

Hogan CJ, Carroll JA, Rohrs HW, Biswas P, Gross ML. 2008. Charge carrier field emission determines the number of charges on native state proteins in electrospray ionization. J Am Chem Soc 130:6926–6927.

Hoyau S, Norrman K, McMahon TB, Ohanessian GA. 1999. Quantitative basis scale of Na+ affinities of organic and small biological molecules in the gas phase. J Am Chem Soc 121:8864–8875.

Ikonomou MG, Blades AT, Kebarle P. 1991. Electrospray mass spectrometry of methanol and water solutions. Suppression of electric discharge with SF_6 gas. J Am Soc Mass Spectrom 2:497–505.

Iribarne JV, Thomson BA. 1976. On the evaporation of small ions from charged droplets. J Chem Phys 64:2287–2294.

Juraschek R, Dulks T, Karas M. 1999. Nanoelectrospray—More than just a minimized-flow electrospray ion source. J Am Soc Mass Spectrom 10:300–308.

Kaltashov IA, Mohimen A. 2005. Estimates of protein areas in solution by electrospray ionization mass spectrometry. Anal Chem 77:5370–5379.

Kauzmann W. 1959. Some factors in the interpretation of protein denaturation. Adv Prot Chem 14:1–63.

Kebarle P, Tang L. 1993. From ions in solution to ions in the gas phase. Anal Chem 65:A972–A986.

Klassen JS, Anderson SG, Blades AT, Kebarle P. 1996. Reaction enthalpies for M + L = M + L, where M = Na+, K+ and L = acetamide, N-methyl acetamide, N,N-dimethylacetamide, glycine, glycylglycine, from determinations of the collision-induced thresholds. J Phys Chem 100:14218–14227.

Loscertales IG, Fernandez de la Mora J. 1995. Experiments on the kinetics of field evaporation of small ions from droplets. J Chem Phys 103:5041–5060.

Loeb L, Kip AF, Hudson GG, Bennet WH. 1941. Pulses in negative point-to-plane corona. Phys Rev 60:714–722.

Loo J. 1997. Studying noncovalent protein complexes by electrospray ionization mass spectrometry. Mass Spectrom Rev 16:1–23.

Marginean I, Parvin L, Heffernan L, Vertes A. 2004. Flexing the electrified meniscus: The birth of a jet in electrosprays. Anal Chem 76:4202–4207.

McMahon TB, Ohanessian G. 2000. An experimental and ab initio study of the nature and binding of gas phase complexes of sodium ions. Chem Eur J 6:2931–2935.

Nesatty VJ, Suter MJF. 2004. On the conformation-dependent neutralization theory and charging of individual proteins and their non-covalent complexes in the gas phase. J Mass Spectrom 39:93–97.

Peschke M, Verkerk UH, Kebarle P. 2004. Features of the ESI mechanism that affect the observation of multiply charged noncovalent complexes and the determination of the association constant by the titration method. J Am Soc Mass Spectrom 15:1424–1434.

Rayleigh L. 1882. On the equilibrium of liquid conducting masses charged with electricity. Phil Mag Ser 5(14):184–186.

Reinhold VN, Reinhold BB, Castello CE. 1995. Carbohydrate molecular weight profiling, sequence, linkage and branching data. Anal Chem 67:1772–1784.

Richardson CB, Pigg AL, Hightower RL. 1989. On the stability limit of charged droplets. Proc Roy Soc London A 422:319–328.

Samalnikova M, Grandori R. 2003. Protein charge state distributions in electrospray ionization mass spectrometry do not appear to be limited by the surface tension of the solvent. J Am Chem Soc 125:13362–13365.

Samalnikova M, Grandori R. 2005. Testing the role of surface tension in protein ionization by mass spectrometry. J Mass Spectrom 40:503–510.

Santos LS, Metzger JO. 2006. Study of homogeneously catalyzed Ziegler–Natta Polymerization of ethene by ESI-MS. Angew Chem Int Ed 45: 977–981.

Schmidt A, Karas M, Dulks T. 2003. Effect of different solution flow rates on analyte signals in nano-ESI-MS, or: When does ESI turn into nano-ESI. J Am Soc Mass Spectrom 14:492–500.

Schweizer JW, Hanson DN. 1971. Stability limit of charged drops. J Colloid Interface Sci 35:417–423.

Shelimov KB, Clemmer DE, Hudgins RR, Jarrold M. 1997. Protein structure in vacuo: Gas phase conformations of BPTI and cytochrome C. J Am Chem Soc 119:2240–2248.

Shou WZ, Naidong W. 2005. Simple means to alleviate sensitivity loss by trifluoroacetic acid (TFA) mobile phases in the hydrophilic interaction chromatography-electrospray tandem mass spectrometric bioanalysis of basic compounds. J Chromatogr B 825:186–192.

Smith DPH. 1986. The electrohydrodynamic atomization of liquids. IEEE Trans Ind Appl 22:527–535.

Smith JN, Flagan RC, Beauchamp JL. 2002. Droplet evaporation and discharge dynamics in electrospray ionization. J Phys Chem A 106: 9957–9967.

Stevenson DP, Schissler DO. 1958. Reactions of gaseous ions molecular ions with gaseous molecules, IV. Experimental method and results. J Chem Phys 29:282–294.

Sun J, Kitova EN, Wang W, Klassen JS. 2006. Method for distinguishing specific from nonspecific protein-ligand complexes in nanoelectrospray ionization mass spectrometry. Anal Chem 78:3010–3018.

Sun J, Kitova EN, Klassen JS. 2007. Method for stabilizing protein–ligand complexes in nanoelectrospray ionization mass spectrometry. Anal Chem 79:416–425.

Taflin DC, Ward TL, Davis EJ. 1989. Electrified droplet fission and the Rayleigh limit. Langmuir 5:376–384.

Takahashi N, Fenn JB. 1992. Electrospray mass spectrometry of poly (ethylene glycols) with molecular weights up to five million. J Am Chem Soc 114:3241–3246.

Tang K, Gomez A. 1995. Generation of monodisperse water droplets from electrosprays in a corona-assisted cone-jet mode. J Colloid Sci 175: 323–326.

Tang L, Kebarle P. 1993. Dependence of the ion intensity in electrospray mass spectrometry on the concentration of the analytes in the electrosprayed solution. Anal Chem 65:3654–3668.

Taylor GI. 1965. The stability of horizontal fluid interface in a vertical electric field. J Fluid Mech 2:1–15.

Thomson BA, Iribarne JV. 1979. Field induced ion evaporation from liquid surfaces at atmospheric pressure. J Phys Chem 71:4451–4463.

Tolic RP, Anderson GA, Smith RD, Brothers HM, Spindler R, Tomalia DA. 1997. Electrospray ionization Fourier transform ion cyclotron resonance mass spectrometric characterization of high molecular mass starburst (TM) dendrimers. Int J Mass Spectrom Ion Proc 165:405–418.

Van Berkel GJ, Zhou F, Aronson JT. 1997. Changes in bulk solution pH caused by the inherent controlled-current electrolytic process of an electrospray ion source. Int J Mass Spectrom Ion Proc 162:55–67.

Verkerk UH, Kebarle P. 2005. Ion-ion and ion-molecule reactions at the surface of proteins produced by nanospray. Information on the number of acidic residues and control of the number of ionized acidic and basic residues. J Am Soc Mass Spectrom 16:1325–1341.

Wampler FW, Blades AT, Kebarle P. 1993. Negative ion electrospray mass spectrometry of nucleotides: Ionization from water solution with SF_6 discharge suppression. J Am Soc Mass Spectrom 4:289–295.

Wang W, Kitova EN, Klassen JS. 2003. Bioactive recognition sites may not be energetically preferred in protein-carbohydrate complexes in the gas phase. J Am Chem Soc 125:13630–13861.

Whitehouse CM, Dreyer RN, Yamashita M, Fenn JB. 1985. Electrospray interface for liquid chromatographs and mass spectrometers. Anal Chem 57:675–679.

Wilm M, Mann M. 1994. Electrospray and Taylor-Cone Theory, Dole's beam of macromolecules at last? Int J Mass Spectrom Ion Proc 136:167–180.

Wilm M, Mann M. 1996. Analytical properties of the nanoelectrospray ion source. Anal Chem 68:1–8.

Winger BA, Light-Wahl KJ, Ogorzalek Loo RR, Udseth HR, Smith RD. 1993. Observations and implications of high mass-to-charge ratio ions from electrospray ionization mass spectrometry. J Am Soc Mass Spectrom 4:536–545.

Wortman A, Kistler-Momotova A, Zenobi R, Heine MC, Wilhelm D, Pratsinis SE. 2007. Shrinking droplets in electrospray ionization and their influence on chemical equilibria. J Am Soc Mass Spectrom 18:385–393.

Yamashita M, Fenn JB. 1984a. Electrospray ion source. Another variation on the free-jet theme. J Phys Chem 88:4451–4459.

Yamashita M, Fenn JB. 1984b. Negative ion production with the electrospray ion source. J Phys Chem 88:4671–4675.

Zhang X, Chen X, Chen P. 2004. Mass spectrometric study of the conversion of rhenium diolates to metallaoxetanes and carbenes Coordination number, polar, and steric effects. Organometallics 23:3437–3447.

Znamenski V, Marginean I, Vertes A. 2003. Solvated ion evaporation from charged water nanodroplets. J Phys Chem A 107:7406–7412.

Paul Kebarle Prof. Emeritus. Chemistry U. Alberta: Kebarle and co-workers starting in the early 1960s, pioneered the field of Atmospheric Pressure and High Pressure Mass spectrometry and particularly the study of ion–molecule reactions at high pressure, their rate and equilibrium constants. This led to the development of the Field of Gas Phase Ion Thermochemistry providing data on proton and electron affinities, Ion Hydration and other Ion Solvation energies. The results proved of significance not only to Gas Phase Ion Chemistry and Mass Spectrometry but also to Ionic reactions in solution and Physical Organic Chemistry. After the discovery and development by Dole and Fenn of Electrospray Mass Spectrometry, Kebarle and co-workers felt very much at home in this area, which amounted to a method with which ions present in solution were being transferred to the gas phase. For this reason and the great potential of ESIMS as an analytical method, they chose to direct much of their research to the study of the Mechanism of Electrospray Mass Spectrometry.

Udo H. Verkerk, Research Associate, Centre for Research in Mass Spectrometry, York University. Dr. Verkerk obtained an MSc in Organic Chemistry at the Free University, Amsterdam, Holland before moving to Canada where he obtained a PhD in Organometallic Chemistry at the University of Alberta, Edmonton. After a brief exposure to mass spectrometry as a postdoc with Paul Kebarle, he continues his mass spectrometry studies at the Centre for Research in Mass Spectrometry, York University focusing on TCID of non-covalent metal complexes and corresponding mass spectrometry hardware development. His main interests are mass spectrometry of non-covalent and supramolecular complexes, fundamentals of ES ionization, MS hardware development and use of mass spectrometry in the study of proteins, enzymes as well as reactive organometallic species.